의학박사 학위논문

Modulation of persistent Na^+ currents by group I metabotropic glutamate receptors in the dendrites of CA1 pyramidal neurons

CA1 피라미드 세포의 수상돌기에서 대사성 글루탐산 수용체에 의한 지속성 Na^+ 전류의 조절

2019 년 2 월

서울대학교 대학원

의과학과 생리학 전공

유 원 진

A thesis of the Degree of Doctor of Philosophy

CA1 피라미드 세포의 수상돌기에서 대사성 글루탐산 수용체에 의한 지속성 Na^+ 전류의 조절

Modulation of persistent Na^+ currents by group I metabotropic glutamate receptors in the dendrites of CA1 pyramidal neurons

Feb 2019

The Department of Physiology,

Seoul National University

College of Medicine

Weonjin Yu

CA1 피라미드 세포의 수상돌기에서 대사성 글루탐산 수용체에 의한 지속성 Na^+ 전류의 조절

지도 교수 호 원 경

이 논문을 의학박사 학위논문으로 제출함

2019년 2월

서울대학교 대학원

의과학과 생리학 전공

유 원 진

유원진의 의학박사 학위논문을 인준함

2018년 12월

위 원 장 _____ (인)

부위원장 _____ (인)

위 원 _____ (인)

위 원 _____ (인)

위 원 _____ (인)

Modulation of persistent Na^+ currents by group I metabotropic glutamate receptors in the dendrites of CA1 pyramidal neurons

by

Weonjin Yu

A thesis submitted to the Department of Physiology in partial fulfillment of the requirements for the Degree of Doctor of Philosophy in Physiology at Seoul National University College of Medicine

Dec 2018

Approved by Thesis Committee:

Professor _____Chairman

Professor _____Vice chairman

Professor _____

Professor _____

Professor _____

ABSTRACT

Modulation of persistent Na^+ currents by group I metabotropic glutamate receptors in the dendrites of CA1 pyramidal neurons

Weonjin Yu

The Department of Physiology

The Graduate School

Seoul National University

College of Medicine

Dendritic Na^+ channels in pyramidal neurons are known to amplify synaptic signals, thereby facilitating action potential (AP) generation. However, the mechanisms that modulate dendritic Na^+ channels have remained largely uncharacterized. Here, I report a new form of short-term plasticity in which proximal excitatory synaptic inputs to hippocampal CA1 pyramidal neurons (CA1-PNs) transiently elevate dendritic excitability. High-frequency stimulations (HFS) to the Schaffer collateral (SC) pathway activate mGluR5-dependent Ca^{2+} signaling in the apical dendrites, which, with calmodulin, upregulates specifically Nav1.6 channel-mediated persistent Na^+ currents ($I_{Na,P}$) in the dendrites. This HFS-induced increase in dendritic $I_{Na,P}$ results in transient increases in the amplitude of excitatory postsynaptic potentials induced by both proximal SC and distal perforant path stimulation, leading to the enhanced probability of AP firing associated with decreased AP thresholds, as well as,

leading to increasing firing rate and advancement of spike timing with an improvement of temporal precision. Taken together, my study identifies dendritic $I_{Na,P}$ as a novel target for mediating activity-dependent modulation of dendritic integration and neuronal output. As mGluR5 activation is induced by physiologically plausible brief high-frequency stimulation at CA3-CA1 synapses, my results also suggest that mGluR5-induced enhancement of dendritic $I_{Na,P}$ in CA1-PNs may therefore provide important implications for our understanding about place field formation in the hippocampus.

Key Words: mGluR5-dependent plasticity, persistent sodium current, CA1 pyramidal neurons, Intrinsic excitability, High-frequency stimulation

Student Number: 2009-21894

CONTENTS

LIST OF FIGURES

LIST OF ABBREVIATIONS

ADP	afterdepolarization
AMPA	α-amino-0033hydroxi-5-methyl-ioxyzole-4-propionic acid
APV	(2R)-amino-5-phosphonopentanoic acid
cADPR	cyclic adenosine diphosphate ribose
CaM	Calmodulin
CA1-PNs	CA1 pyramidal neurons
DMSO	dimethyl sulfoxide
EPSC	excitatory postsynaptic current
EPSP	excitatory postsynaptic potential
HFS	High-frequency stimulation
mGluR	Metabotropic glutamate receptor
MPEP	2-methyl-6-(phenylethynyl) pyridine
NMDA	*N*-methyl-*D*-aspartate
$I_{Na,P}$	persistent sodium currents
$I_{Na,T}$	transient Na^+ current
PTX	picrotoxin

RS-DHPG	(RS)-3,5-Dihydroxyphenylglycine
SC synapse	Schaffer Collateral synapse
RyR	ryanodine receptor

INTRODUCTION

The processes that excitatory postsynaptic potentials (EPSPs) cause postsynaptic neurons to evoke action potentials (APs) are the basis to the operation of neural network. Bliss and Lomo (1) found that in hippocampus EPSPs increased in amplitude after high frequency stimulation (HFS), and potentiated EPSPs often generate APs more effectively than would be expected from the increase in EPSP amplitude alone, suggesting a higher efficiency of EPSP-spike coupling after HFS and intrinsic excitability also has plastic properties. This type of intrinsic plasticity was termed EPSP-to-spike (E-S) coupling or E-S potentiation. Several factors may contribute to this type of plasticity, including changes in resting and threshold potentials of postsynaptic cells. Spike initiation may also depend on the changes in somatic or dendritic membrane conductances (2). In CA1-PNs, a localized decrease in dendritic A-type K^+ currents after HFS stimulation may also contribute to the enhancement of excitability (3). On the other hand, neuronal excitability may be decreased by HFS that seemed to result from increased I_h (4). These ion channel can be regulated in an activity-dependent manner, which provides a key mechanism of intrinsic plasticity (3, 5, 6). Given a variety of voltage-gated conductances in PN dendrites, exploring how active dendrites process incoming synaptic signals and transform them into APs is essential groundwork for understanding brain functions (7, 8). Hippocampal E-S potentiation has been reported after mGluR stimulation (9), but the contribution of increased neuronal excitability has not been clearly

demonstrated.

The group I metabotropic glutamate receptors(mGluRs) are known to be important for regulating a variety of ion channels, leading to the alteration of neuronal excitability by regulation of ion channels, including nonselective cation channels, K^+ channels, and Na^+ channels (10-13). These ion channels are heterogeneously distributed along the somatodendritic axis of CA1 neurons (14-16). Especially, a gradual decrease in Nav1.6 density along the proximodistal axis of the CA1 dendrite has been described by EM immunolocalization study (17). Moreover, mGluR5 is mainly expressed in dendritic fields of the stratum radiatum in hippocampus, and subcellularly, Group I mGluRs are localized postsynaptically in a perisynaptic zone surrounding the ionotropic receptors (18). Given heterogeneous distribution of voltage-gated ion channels and mGluR5 are heterogeneously distributed along the somatodendritic axis, mGluR5 activation by synaptic or pharmacological stimulation should have distinct effects depending on the location of apical dendrites of the CA1-PNs.

The persistent Na^+ current ($I_{Na,P}$) is a subthreshold regenerative conductance with a more negative activation voltage than transient Na^+ current ($I_{Na,T}$) and has slowly inactivating characteristics (19). $I_{Na,P}$ is believed to play critical roles in AP initiation, synaptic integration, and afterpotentials (20). It has been reported that absence of Nav1.6 reduces the persistent Na^+ current (21) and group I mGluRs regulate $I_{Na,P}$ in CA1-PNs (22). Moreover, $I_{Na,P}$ in Purkinje cells and CA1-PNs can be activated by EPSPs (23).

Therefore, activation of group I mGluRs may modulate dendritic $I_{Na,P}$ in CA1-PNs.

It is possible that the intracellular Ca^{2+} signal released by HFS, which cause regulation of dendritic Ca^{2+} channel conductances (24), might initiate signaling cascades that also regulate a variety of ionic conductances on dendrites. As Nav1.6 currents can be selectively modulated by Ca^{2+}/CaM (25), synaptic activation of mGluR5 during HFS may modulate dendritic $I_{Na,P}$ in CA1-PNs.

The hippocampus is a major part of the brain responsible for spatial learning and memory. When animals navigate large environments, a subset of hippocampal pyramidal neurons termed 'place cells' encode the spatial information. Recent study has examined the modulation of intrinsic excitability in the formation of place field in CA1- PNs. During spatial navigation, CA1-PNs that later become place cells showed a lower AP threshold and an increased intrinsic excitability convert silent CA1-PNs receiving excitatory inputs from other spatially tuned neurons into functional firing place cells (26-29). These results imply the importance of the modulation of the components that influence the firing ability of CA1-PNs.

In the present study, I provide the novel mGluR-mediated mechanisms of modulating firing property of CA1-PNs. Activation of mGluRs by HFS of SC inputs can transiently modulate dendritic excitability of postsynaptic neurons. Using combined electrophysiological and Ca^{2+} fluorescence recordings in acute hippocampal slices, I show that HFS induces Ca^{2+} release in the dendrites of CA1-PNs via activation of group I mGluRs. This Ca^{2+}

signal enhances dendritic $I_{Na,P}$, which in turn increase synaptic responses induced by physiologically relevant stimulation and consequently increases the probability to generate APs. Moreover, Selective modulation of $I_{Na,P}$ in the proximal apical dendrites of CA1-PNs leads to increased firing frequency, advancement of spike timing, and improvement of temporal precision during behaviorally relevant oscillation. Given that mGluR5 can be activated by physiologically relevant network condition (30), I propose that the activation of mGluRs may represent one of key cellular mechanisms for determining place cell firing.

Materials and Methods

Animals and ethical approval. All animal studies and experimental protocols were approved by the Institutional Animal Care and Use Committee (IACUC, approval No. SNU-090115-7) at Seoul National University. The animals were maintained in standard environmental conditions (25 ± 2 °C; 12/12 h dark/light cycle) and were housed under veterinary supervision at the Institute for Experimental Animals, Seoul National University College of Medicine. mGluR5 K/O mice were purchased from the Jackson laboratory (Maine, USA).

Hippocampal slice preparation. Hippocampal slices were prepared from Sprague–Dawley rats (P11–P19; P9–P16 for the experiments in Figure 4) or C57BL/6 mice (P16–P20; experiments on mGluR5 K/O mice) of either sex. After rats or mice were anaesthetized by inhalation of 5% isoflurane, they were decapitated and the brain quickly removed and chilled in an ice-cold high-magnesium cutting solution containing the following (in mM): 110 choline chloride, 25 $NaHCO_3$, 20 Glucose, 2.5 KCl, 1.25 NaH_2PO_4, 1 Sodium pyruvate, 0.5 $CaCl_2$, 7 $MgCl_2$, 0.57 Ascorbate, with pH adjusted to 7.4 by saturating with carbogen (95% O2, 5% CO2), and with osmolality of approximately 300 mOsm/L. The isolated brain was glued onto the stage of a vibrating blade microtome (Leica VT1200) and 300 μm-thick transverse hippocampal slices were cut. The slices were incubated at 34 °C for 30 min in the artificial cerebrospinal fluid (aCSF) containing the following (in mM): 125 NaCl, 25 $NaHCO_3$, 20 Glucose, 2.5 KCl, 1.25 NaH_2PO_4, 1 Sodium pyruvate,1 $CaCl_2$, 0.5 $MgCl_2$, 0.57 Ascorbate, bubbled with 95% O_2 and 5% CO_2., and thereafter

maintained at room temperature.

Electrophysiological recordings. Whole-cell voltage- or current-clamp recordings from hippocampal CA1-PNs (one cell per slice) were performed at 32 ± 1°C and the rate of aCSF perfusion was maintained at 1–1.5 ml min^{-1}. The recordings were made in somata with EPC-10 amplifier (HEKA Electronik) at a sampling rate of 10–50 kHz. For current-clamp recordings, the membrane potential was held at the resting membrane potential (RMP). Patch pipettes (3–4 MΩ) for current clamp mode were filled with internal solutions containing the following (in mM): 130 Potassium gluconate, 20 KCl, 10 Na_2-Phosphocreatine, 10 HEPES, 2 MgATP, 0.3 NaGTP, 0.1 EGTA. To isolate $I_{Na,P}$ in whole-cell voltage-clamp recordings, we used a modified aCSF containing 20 mM tetraethylammonium chloride (TEA) and 0.2 mM $CdCl_2$ with internal solutions containing the following (in mM): 120 Cs-methane sulphonate, 10 CsCl, 10 TEA-Cl, 1 $MgCl_2$, 10 HEPES, 0.1 EGTA, 0.4 Tris-GTP, 3 Mg-ATP, and 5 Na_2-phosphocreatine (293 mOsm, pH 7.3 with CsOH). For some cases, the apical dendrite of the neuron was cut by a blade under the microscope. Monopolar electrodes (tip size: 5-10 μm) filled with aCSF were connected to the stimulator (Master-8, AMPI, Jerusalem, Israel) to deliver HFS or TBS. We recorded series resistance throughout experiments, and excluded neurons with series resistance > 20 MΩ from data analysis. Membrane potential values were presented as recorded without correcting liquid junction potentials. Neurons with resting potentials more positive than −55 mV were discarded.

For local application of drugs, a pneumatic pump (Toohey Spritzer)

was used with a puffing glass pipette (tip size: 1.5–2 μm). The puff area was determined from the fluorescence profile of Alexa Fluor 488 (100 μM, Invitrogen), which was added to the puffing pipette. The ejection pressure was adjusted (typically to 0.5–1 psi) such that the puff area became a circular region that diameter was 20 μm from the center (the puffing pipette tip) at 2 s after the start of ejection. Recordings obtained between 3-5 min after the start of drug ejection were regarded to represent drug effects.

Gene knock-down using RNA interference. A short-hairpin RNA (shRNA) to deplete endogenous Scn8a from the hippocampal CA1-PN was used in an organotypic slice culture. Scn8a-targeting short-interfering (si) RNA (5′-CAAGAGGTTTCTGCATAGA-3′, shNav1.6) and non-targeting siRNA control (shCTRL) were purchased from GeneCopoeia. CA1-PNs in the cultured slices at DIV5–6 were transfected with plasmids encoding shNav1.6/GFP or shCTRL/GFP using the biolistic transfection methods (Helios Gene Gun System, BioRad). The transfected CA1-PNs were subject to electrophysiological recording 5 days after the transfection. The resting membrane potential and the AP threshold were -64.54 ± 0.97 mV, -42.04 ± 1.07 mV for shCTRL and -65.6 ± 1.19 mV, -47.7 ± 2.27 mV for shNav1.6, respectively.

Calcium measurements. The procedures for cytosolic Ca^{2+} measurement in brain slices were previously described in detail (31). For fluorescence excitation, we used a polychromatic light source (xenon-lamp based, Polychrome-IV; TILL-Photonics), which was coupled to the epi-illumination

port of an inverted microscope (IX70, Olympus) via a quartz light guide and a UV condenser. Microfluorometry was performed with a 40x water immersion objective (NA 1.15, UAPO 406 W/340, Olympus) and a photodiode (TILL-Photonics). Fluorescence intensity at an ROI including the dendrite was measured at 10 Hz with double-wavelength excitation at 340 nm (F_{340}) and 380 nm (F_{380}). The ratio $R = F_{340}/F_{380}$ was converted to $[Ca^{2+}]_i$ values according to the following equation: $[Ca^{2+}]_i = K_{eff} (R - R_{min})/(R_{max} - R)$, where K_{eff} was estimated as 0.93 μM. Calibration parameters determined by using *ex-vivo* calibration were typically 0.24 for R_{min} and 3.4 for R_{max}.

Drugs. (*RS*)-3,5-DHPG, LY367385, MPEP, CNQX, APV, picrotoxin, ryanodine, TTX, riluzole were purchased from Tocris Bioscience. Choline chloride was Junsei Chemical (Tokyo, Japan). U73122 was from Biomol. Fura 2 and 8-NH_2-cADPR were from Molecular Probes. All other drugs were purchased from Sigma-Aldrich. Stock solutions of drugs were made by dissolving in deionized water or DMSO according to manufacturer's specifications and were stored at -20°C. On the day of the experiment one aliquot was thawed and used. The concentration of DMSO in solutions was maintained at 0.1%.

Experimental design and statistical analysis. All data were presented as mean ± standard error of the mean (SEM). Statistical analysis was performed using IgorPro (version 6.1, WaveMetrics) and OriginPro (version 9.0, Microcal). Wilcoxon signed-rank test and Mann-Whitney test were used as appropriate to compare paired and non-paired groups, respectively. P-values of < 0.05 were

considered statistically significant.

Results

HFS of SC pathway induces mGluR5-mediated Ca^{2+} release at proximal apical dendrites of hippocampal CA1 pyramidal neurons

I first tested the effects of a group I mGluR on the dendrites of hippocampal CA1-PNs. I applied HFS (100 Hz for 0.5 s) to SC synapses paired with backpropagating action potentials (bAPs), which are known to evoke group I mGluR-mediated Ca^{2+} signals in the hippocampal CA1-PN dendrites (32). To prevent long-term synaptic plasticity mediated by NMDA receptors and the recruitment of GABAergic inhibition, all the experiments were performed in the presence of APV (50 μM) and PTX (100 μM) in the bath. To measure Ca^{2+} transients in dendrites, cells were loaded with the high-affinity Ca^{2+} indicator dye Fura-2 (100 μM; Fig. 1Aa). SC fibers that terminate on proximal dendrites were activated by a stimulation electrode positioned at ~100 μm away from the soma and ~50 μm away from the trunk of the apical dendrite (Fig. 1Aa). HFS to the SC pathway at subthreshold intensities did not increase Ca^{2+}, whereas the same subthreshold synaptic stimulations when combined with somatic current injections or suprathreshold synaptic stimulation without somatic current injections that are sufficient to elicit two or three APs, induced a large transient increase of Ca^{2+} in the proximal dendrites (Fig. 1Ab; (32). These protocols were further pharmacologically corroborated by brief puffs of DHPG (250 μM), a group I mGluR agonist at 30 s intervals, to the apical dendrites, yielding a similar Ca^{2+} transient (Fig. 1Ac).

I next dissected the specific subtypes of group I mGluR involved in HFS-induced Ca^{2+} transients. HFS-induced Ca^{2+} transients were not affected by the mGluR1 antagonist LY367385 (25 μM) but were substantially abolished by the mGluR5 antagonist MPEP (10 μM; Fig. 1Ba,C). Dependence of HFS-induced Ca^{2+} transients on mGluR5 activation was further confirmed using mGluR5 knockout (K/O) mice (33). In the hippocampal slices obtained from wild-type (WT) mice, HFS to SC pathway induced large Ca^{2+} transients in the apical dendrites of CA1-PNs, but no Ca^{2+} transients were induced by the same stimulation in the slices obtained from mGluR5 K/O mice (Fig. 1Bb,C). Together, these results indicate that the HFS to proximal SC synapses induces mGluR5-dependent Ca^{2+} release in the apical dendrites of CA1-PNs.

To further elucidate the mechanisms of HFS-induced Ca^{2+} transients, I systematically analyzed the downstream signaling pathways. Group I mGluR is well-known to induce Ca^{2+} release from intracellular stores via phospholipase C (PLC)/inositol-3,4,5-triphosphate (IP3)-dependent pathway (34, 35). However, application of U73122 (a PLC inhibitor) to the bath solutions or inclusion of heparin (an IP3 receptor inhibitor in the pipette solutions) did not reduce HFS-induced Ca^{2+} release (Fig. 1D,E). Rather, HFS-induced Ca^{2+} release was abolished when cyclic adenosine diphosphate ribose (cADPR)/ryanodine receptor (RyR) pathway was blocked by the inclusion of 8-NH2-cADPR, nicotinamide, or ryanodine in the pipette solutions (Fig. 1D,E), consistent with our previous reports (36). Therefore, these results confirmed

that HFS of the SC pathway readily induced mGluR5 activation and Ca^{2+} release from the intracellular store, which was mediated by cADPR.

HFS at SC pathway causes post-tetanic potentiation of EPSP-spike coupling

To test the role of HFS-induced Ca^{2+} release in the regulation of neuronal function in CA1-PNs, I studied the effects of HFS on excitatory postsynaptic currents (EPSCs) and excitatory postsynaptic potentials (EPSPs) evoked by SC stimulations. HFS did not induce any significant change in the amplitude or paired pulse ratio of the EPSCs (Fig. 2A,B). In contrast, the amplitude of EPSPs was significantly increased after HFS (Fig. 2A,B), indicating that HFS affects dendritic excitability but not the efficacy of synaptic transmission. I also verified that the resting membrane potentials remained unchanged after HFS (control: -65.2 ± 0.5 mV, after HFS: -65.1 ± 0.4, n = 8; p = 0.38). To further examine the effects of HFS on postsynaptic excitability, I probed whether HFS leads to changes in spiking activity in response to high-frequency input from CA3 (30); Fig. 2C). I repeated high-frequency burst stimulation (5 stimuli at 100 Hz) of SC fibers at 10 sec intervals before and after HFS. HFS of the SC inputs readily induced increases in spike probability (Before HFS: 0.25 ± 0.02, after HFS: 0.7 ± 0.03, n = 16; $p < 0.001$; Fig. 2C). I refer to this form of intrinsic plasticity as post-tetanic E-S (EPSP-to-spike) potentiation (PT-ESP). PT-ESP was accompanied by a large increase in the mean amplitude of EPSPs (Fig. 2D). Furthermore, the threshold voltage (V_{th}) for AP firing (defined as the voltage at which dV/dt exceeded 20 V/s) was hyperpolarized by

-0.89 ± 0.7 mV (n = 8, $p < 0.01$) after HFS (Fig. 2E), suggesting the involvement of Na^+ channels. Maximum dV/dt during APs which represents axosomatic Na^+ channel activity was unchanged after HFS (Fig. 2E). Considering that HFS evoked local dendritic Ca^{2+} signals that were not propagated into soma, these results suggest that enhancement of dendritic Na^+ channels contributes to HFS-induced E-S potentiation.

To investigate whether dendritic Na^+ channels are responsible for HFS-induced E-S potentiation, I examined the effect of HFS under the condition that dendritic Na^+ channels are reduced. Low concentration of tetrodotoxin (TTX; 10 nM) was often used for block of the dendritic Na^+ channels without affecting synaptic transmission (37, 38). In the presence of 10 nM TTX, PT-ESP was completely abolished (Fig. 2F). As predicted, the amplitude of EPSPs were not affected by HFS (Fig. 2G) and the AP threshold remained unchanged (Fig. 2H). These results indicate that dendritic Na^+ channels are important for PT-ESP.

HFS-induced PT-ESP requires mGluR5-dependent Ca^{2+} signaling and is mediated by persistent Na^+ currents

To quantify the effects of PT-ESP under situations that more closely resemble the physiological network activity, we applied high-frequency burst stimulation repeated six times at 4 Hz that mimics the endogenous theta rhythm (Theta burst stimulation, TBS) in the hippocampus (4–10 Hz) during exploratory behavior. Stimulus intensity was set to be slightly over the threshold for the first

burst stimulation, resulting in subthreshold or the firing of one or two APs during second to sixth bursts. In the presence of APV and PTX, the number of spikes per sweep (Repeated every 5 sec; Fig. 3A) was maintained at the constant level, indicating that TBS in our experimental condition did not have potentiating effects on AP generation. However, HFS of the SC inputs reliably produced PT-ESP (red; $n = 9$; $p < 0.005$; Fig. 3A,B). To investigate the duration of the HFS effect on AP generation, I counted the number of APs during TBS and plotted them as a function of time ($n = 9$; Fig. 3B). The increase in AP number following HFS did not last long and decreased gradually to the basal level within 2 min (Fig. 3B). When I repeated the HFS, similar increases in AP firing were observed (Fig. 3B).

I next examined the dependence of HFS-induced PT-ESP on mGluR5 activation. As expected, PT-ESP was abolished in the presence of MPEP ($n = 6$; $p < 0.005$; Fig. 3C), whereas no changes were detected during the bath application of LY367385 ($n = 6$; $p = 0.81$; Fig. 3C). PT-ESP was also abolished when 10 mM BAPTA was included in the whole-cell patch pipette to inhibit a rise in cytosolic Ca^{2+} (Fig. 3E), indicating the involvement of mGluR5-dependent Ca^{2+} release in PT-ESP. In addition, PT-ESP was completely abolished by inhibiting calmodulin (CaM)-mediated signaling by using CaM inhibitory peptides (Fig. 3F). I then tested several additional blockade to identify the mechanism of mGluR5-dependent Ca^{2+} release required for PT-ESP, confirming the involvement of cADPR/RyR pathway (Fig. 3G–I). Finally, the necessity of mGluR5 in PT-ESP was examined using mGluR5 K/O mice. In

WT mice, HFS at SC synapses induced PT-ESP to similar degrees as observed in rat hippocampus but not in mGluR5 K/O mice (Fig. 3D). Altogether, these results suggest that mGluR5-dependent Ca^{2+} release activates Ca^{2+}/CaM signaling leading to PT-ESP.

To identify the ionic mechanisms underlying PT-ESP, I tested the pharmacological blockers that inhibit the ion channels underlying mGluR-mediated events (Fig. 3J,K). It was previously reported that group I mGluR agonist enhances R-type Ca^{2+} currents resulting in the generation of afterdepolarization in CA1-PNs (39). Thus, I examined the involvement of R-type Ca^{2+} channels in PT-ESP by using a specific blocker SNX-482. PT-ESP was not prevented in the presence of SNX-482 ($p = 0.09$; Fig. 3J). Another candidate is the persistent Na^+ currents ($I_{Na,P}$) that are increased by DHPG in medium spiny neurons of nucleus accumbens (40). $I_{Na,P}$ has been shown to amplify EPSPs and facilitate repetitive firing in CA1-PNs (41, 42). Therefore, I examined the effect of a $I_{Na,P}$ blocker, riluzole (43), on PT-ESP. In the presence of riluzole (10 μM), PT-ESP was completely abolished (Fig. 3K), which is in agreement with my observation that low concentration of TTX can block PT-ESP (Fig. 2F; (44)). I therefore hypothesized that HFS may induce potentiation of $I_{Na,P}$, which in turn leads to PT-ESP.

mGluR5 activation upregulates persistent Na^+ currents

To test this hypothesis, I examined the relationship between the modulation of

$I_{Na,P}$ and the activation of mGluR5 in CA1-PNs. $I_{Na,P}$ was recorded using a slowly rising voltage ramp pulse (50 mV/s) from a holding potential of −60 mV to 0 mV in voltage-clamp configuration with Cs^+-based pipette solutions to inhibit K^+ currents (Fig. 4). The mean amplitude of the peak inward current was -126.7 ± 9.6 pA (n = 12) in control conditions but was significantly reduced in the presence of riluzole (-26.4 ± 2.4 pA; n = 14), indicating that the inward current recorded by this protocol represents $I_{Na,P}$ (Fig. 4A,Cb). When I added DHPG to the control bath solution, the peak $I_{Na,P}$ was increased significantly to -178.3 ± 14.1 pA (n = 12), but the addition of DHPG had no effects on the peak $I_{Na,P}$ when cells were pretreated with riluzole (Fig. 4A,Cb). Furthermore, voltage for half-activation of $I_{Na,P}$ ($V_{1/2}$) was hyperpolarized by -3.43 ± 1.34 mV (n = 8) in the presence of DHPG (Fig. 4Ca). These results indicate that group I mGluR-induced potentiation of $I_{Na,P}$ in CA1-PNs leads to the increased amplitude and the reduced activation threshold. I also examined the signaling mechanisms that are involved in DHPG-induced $I_{Na,P}$ potentiation. I found that the DHPG effect was abolished in the presence of MPEP, BAPTA (10 mM), cADPR inhibitors, and CaM inhibitory peptide in the pipette solutions, but not by inhibitors for PLC/IP3 pathway (Fig. 4A,B,Cb), confirming that $I_{Na,P}$ in the CA1-PNs is potentiated by mGluR5-dependent Ca^{2+} signaling.

mGluR5-induced potentiation is mediated by upregulation of dendritic $I_{Na,P}$

To determine whether mGluR5 signaling affects uniformly along the somatodendritic axis or selectively targets somatic or dendritic $I_{Na,P}$, I used the local application of DHPG. The local application of DHPG into the soma did not change the amplitude of $I_{Na,P}$ (Fig. 5A,C). In contrast, the same puff application to the proximal dendrites resulted in moderate increase in $I_{Na,P}$ (Fig. 5A,C). These results indicate that mGluR5 signaling selectively targets dendritic $I_{Na,P}$. Consistent with this idea, bath application of DHPG did not increase $I_{Na,P}$ when the apical dendrites were truncated (~50 μm from the soma; Fig. 5A,C). In addition, in the presence of low TTX (10 nM), the amplitude of $I_{Na,P}$ did not increase after bath application of DHPG ($n = 5$; $p = 0.62$; Fig. 5B,C). Together, these results suggest that mGluR5-dependent Ca^{2+} signals can potentiate $I_{Na,P}$ channels selectively in the dendrites.

To further confirm that mGluR5-dependent potentiation of dendritic $I_{Na,P}$ underlies PT-ESP, I used the local puff applications of riluzole (50 μM) to the dendritic or somatic area. PT-ESP was significantly abolished by a block of dendritic $I_{Na,P}$, but not by those in perisomatic regions (Fig. 5D). Thus, modulation of dendritic $I_{Na,P}$ induced by HFS is the underlying ionic mechanism of PT-ESP.

Dendritic Nav1.6 is a target for mGluR5-dependent upregulation of $I_{Na,P}$

I also tested whether mGluR5-dependent $I_{Na,P}$ enhancement involves a specific

isoform of Na^+ channels. Because Nav1.6 is abundantly expressed in the CA1-PN dendrites (17), I used hippocampal slice culture for downregulating Nav1.6 expression level by shNav1.6 transfection (Fig. 6A). DHPG-induced increase in $I_{Na,P}$ is completely abolished in neurons that are biolistically transfected with plasmid encoding Nav1.6-targeting short hairpin RNA (shNav1.6) but not in neurons transfected with nontargeting RNA (shCTRL, $p < 0.05$; shNav1.6, $p = 0.13$; Fig. 6B). Finally, HFS failed to induce PT-ESP when CA1-PNs were transfected with shNav1.6 (shCTRL, $p < 0.05$; shNav1.6, $p = 0.95$; Fig. 6C,D). Taken together, these results indicate that dendritic Nav1.6 is the target of mGluR5-dependent $I_{Na,P}$ regulation and HFS induced PT-ESP.

HFS at SC pathway causes E-S potentiation at PP synapse

Finally, I examined whether HFS at proximal synapses alone can potentiate EPSPs generated at distal synapses and subsequently boost the AP generation. To this end, a second stimulating electrode was placed more than 150 μm away from the first electrode, while the location of the first stimulating electrode for HFS was unchanged. PT-ESP at distal synapses was robustly induced when HFS was delivered to the proximal synapses (Fig. 7Aa,Ab,C). However, HFS to the same distal synapses did not induce PT-ESP (Fig. 7Ba,Bb,C). Together, these results demonstrate that HFS-induced increases of dendritic excitability occur only at the proximal dendrites and their potentiating effects also affect distal excitatory signals, leading to E-S potentiation of PP inputs.

HFS-induced mGluR activation causes increases in AP firing and its temporal precision

I recently reported that high-frequency stimulations (HFS; 100 Hz for 0.5 s) to Schaffer Collateral (SC) synapses trigger mGluR-dependent Ca^{2+} release in apical dendrites of CA1-PN, which in turn induce calmodulin-dependent increase in persistent Na current ($I_{Na,P}$) that leads to E-S potentiation (22). To investigate the effects of dendritic $I_{Na,P}$ increases on intrinsic excitability of CA1-PNs, I tested whether action potential firing in CA1-PNs evoked by depolarizing current injection is affected by HFS. To rule out any NMDA receptor-dependent changes or the recruitment of GABAergic inhibition, I performed this experiment in the presence of APV (50 μM) and PTX (100 μM) in the bath. I adjusted the current amplitude so that the AP number during 1-s depolarization was between 6 and 8 under control conditions and repeated this stimulation at 10 s interval (Fig. 8A and B). I then applied HFS through a stimulation electrode which was positioned at 80~100 μm away from the soma. After HFS to the SC pathway, there was no change in resting membrane potential (RMP; control: –64.31 ± 0.55 mV, after HFS: –64.25 ± 0.61 mV, n = 8), but AP number increased significantly (Fig. 8A and B). To examine the time course of the HFS effect on intrinsic excitability, I plotted the number of APs as a function of time (Fig. 8B). The increase in AP numbers following HFS did not last long and the increased AP numbers decreased gradually to the basal level within 2 min (Fig. 8B), which is consistent with the effect of HFS on E-S

potentiation reported in our previous paper (22).

As a mechanism for HFS-induced increases in intrinsic excitability, I examined the involvement of $I_{Na,P}$ using $I_{Na,P}$ blocker riluzole (43). In the presence of riluzole (10 μM), HFS-induced increases in AP number were abolished (Fig. 8A and B). These results support the idea that HFS-induced enhancement of dendritic $I_{Na,P}$ facilitates AP firing. I previously showed that HFS-induced enhancement of dendritic $I_{Na,P}$ is mediated by mGluR5 activation (22), and confirmed here that HFS-induced increases in AP number were indeed abolished in the presence of mGluR5 blocker MPEP (Fig. 8D). However, afterhyperpolarization (AHP) following repetitive APs was affected neither by HFS nor by riluzole (Fig. 8A and C).

To further investigate the physiological relevance of $I_{Na,P}$ enhancement on neuronal excitability, I examined the effect of HFS on firing activity of APs evoked by a slow current ramp (250 pA/ 350 ms; Fig. 9). Voltage responses obtained by applying the same ramp for 10 times were superimposed (Fig. 9A), and the effects of HFS on the spike onset time and jitters were analyzed (Fig. 9B). The spike onset time was measured by the duration from the initiation point of the ramp to the first AP. After HFS, spike onset time was advanced by 6.5 ± 2.0 ms (n = 3), but this advancement did not occur in the presence of riluzole (Fig. 9A and B). Spike timing jitter, which represents spike timing precision, was quantified as the standard deviation of the spike onset latencies which were measured while the same ramp was applied for 10 times. The spike timing jitter in control was 2.0 ± 0.3 ms (n = 3), while it decreased to 1.2 ± 0.4

ms after HFS, and this decrease was also reversed by riluzole (Fig. 9A and B). These results suggest that HFS-induced enhancement of $I_{Na,P}$ not only shortens the spike timing but also increases the temporal precision. To investigate how increased $I_{Na,P}$ affect both spike timing and temporal precisions, I further analyzed the threshold for spike initiation during a slow depolarizing current ramp (Fig. 9C and D). The somatic spike threshold was not significantly changed (control: –41.5 ± 1.0 mV; after HFS: –42.0 ± 1.2 mV, n = 3), while the rate of membrane depolarization exhibited prominent changes on the later phase of a slow ramp injection (Fig. 9C), which might account for the facilitation of AP generation and a decrease in spike jitter.

To mimic more physiological voltage responses occurring in vivo (45, 46), I injected an oscillating sine wave current with theta frequency (5 Hz) via somatic pipette, while current amplitudes were adjusted to evoke APs at 5^{th} or 6^{th} sine wave. Representative voltage traces obtained in responses to the injection of 8 sine waves were superimposed (Fig. 9E). After HFS, AP firing was advanced so that 1^{st} AP was evoked at 3^{rd} or 4^{th} sine wave. To examine the effect of HFS on AP onset time, I measured AP onset at 7^{th} sine wave (indicated by a grey box, Fig. 9E). The onset time was reduced by 12.1 ± 1.0 ms and spike timing jitter was also significantly reduced (n = 3, Fig. 9F). These results suggest that activity-dependent advancement of AP firing and increased temporal precision may play a role during the realistic network oscillation.

Group I mGluR-dependent changes in the intrinsic excitability of CA1-PNs

It is well known that group I mGluR activation affects intrinsic excitability in a variety of neuronal types in the brain (40, 47), including hippocampus (48). To compare the effects of HFS-induced mGluR activation with those of global mGluR activation on intrinsic excitability, I examined the effect of bath application of an agonist for group I mGluRs, DHPG, on intrinsic excitability. Intrinsic excitability was assessed by applying 1-s depolarizing current steps with varying magnitude in the presence of synaptic blockers (50 μM APV and PTX 100 μM PTX). CA1-PNs in control conditions showed tonic firing followed by AHP in response to a depolarizing current injection (Fig. 10A), and firing frequency and AHP increased as the magnitude of current increased (Fig. 10B and C). I next applied DHPG (50 μM) into the bath. Application of DHPG gradually depolarized the RMP from –62.9 ± 1.6 mV (n = 7) to –56.9 ± 1.7 mV (n = 7; Fig. 10D). To minimize the effect of RMP changes on spike frequency, I applied depolarizing step pulses after injecting currents to adjust the RMP to match control values (Fig. 10A). DHPG caused a significant increase in the number of APs at all applied current amplitudes (Fig. 10A and B). I also observed generation of afterdepolarization (ADP) following repetitive firing in the presence of DHPG (Fig. 10A and C). I next determined whether the DHPG effects on intrinsic excitability is mediated by mGluR5 activation. DHPG-induced changes in intrinsic excitability were reversed by mGluR5 antagonist MPEP (Fig. 10E–G), but not by mGluR1 antagonist LY367385 (Fig. 10F and G).

To detect the location of the target ion channel mechanisms responsible for mGluR5-induced changes in neuronal excitability, DHPG was applied locally by pressure application from a glass pipette into the dendritic or perisomatic region (Fig. 11A). Interestingly, only the dendritic puff application of DHPG cause the instantaneous increase in firing rates whereas the somatic puff did trigger changes in spiking frequency (Fig. 11B). I next examined the effect of DHPG on truncated CA1-PNs. Consistent with the finding from (Fig. 11A, B), bath application of DHPG did not increase firing frequency when the apical dendrites were truncated (~50 μm from the soma, Fig. 11C, 11D). Averaged number of spikes at 80 pA currents injection was increased in truncated CA1-PNs (intact cells, 14.9 ± 1.0, n = 16; truncated cells, 18.8 ± 2.6, n = 5). Removal of apical dendrite was also accompanied by hyperpolarization in RMP (intact cells, –62.9 ± 1.6 mV, n = 7; truncated cells, -68.2 ± 1.9, n = 5), however, application of DHPG did not depolarize the RMP (Control, -68.2 ± 1.9 mV; DHPG, -66.8 ± 1.6 mV, n = 5, Fig. 12F; n.s., $P > 0.05$). Spike adaptation refers to the progressive slowing of spike frequency following an initial high frequency of spikes during the period of excitation and is also called spike accommodation. In CA1-PNs, this adaptation pattern was clearly observed in response to sustained injections of depolarizing rectangular currents (Fig. 10A, Fig. 11E). Interestingly, spike adaptation was abolished both on dendrite truncation and on DHPG application, and application of DHPG did not increase spike number of truncated CA1-PNs (Fig. 11E). To further investigate the effect of DHPG, I examined the effect of DHPG on APs evoked by current ramp (250 pA/1 sec).

After application of DHPG on intact CA1-PNs, spike onset time was decreased by 78 ± 4 ms (Fig. 11G and 11I, n = 5), but this change did not occur in the truncated CA1-PNs (Fig. 11H and 11I). Taken together, it can be suggested that global activation of mGluR5 targets multiple ion channels to cause diverse effects such as RMP depolarization, increased firing frequency, ADP generation, and decrease of onset time while local activation of mGluR5 by HFS targets dendritic $I_{Na,P}$ selectively to modulate AP firing and its temporal precision.

I further examined the role of $I_{Na,P}$ in DHPG effects using riluzole. Among DHPG effects, RMP depolarization (–55.5 ± 1.3 mV, n = 4) and ADP generation were not affected by riluzole, while increased AP firing was completely reversed by riluzole (Fig. 12A, B and C). To determine the cellular location where $I_{Na,P}$ modulation leads to increased AP firing, I employed the local puff applications of riluzole (50 μM) to the dendritic or perisomatic area in the presence of DHPG. DHPG-induced increases in AP firing was substantially inhibited by a block of dendritic $I_{Na,P}$ (Fig. 12D), but not by block of $I_{Na,P}$ in perisomatic regions (Fig. 12E). These results together with the effects of HFS support the idea that enhancement of dendritic $I_{Na,P}$ mediated by group I mGluR activation is the underlying ionic mechanism of the increased AP firing.

I recognized that ADP generation in response to local application of DHPG to soma or proximal dendrites was not as significant as was observed in bath application of DHPG. Thus, ADP generation by DHPG local application

was further examined including DHPG application to the distal dendrites. ADP induced by DHPG shown in Fig. 10A that lasts a few hundred milliseconds is often referred to as a medium ADP (mADP). I analyzed not only mADP, but also slow ADP (sADP) that lasts for seconds. To exclude the influence of AP frequency changes on ADP, the effect of DHPG on ADP was tested by examining responses to bursts of action potentials evoked by five brief (1 nA, 3 ms, 100 Hz) current injections. The amplitude of mADP was quantified at a fixed time, corresponding to the peak of the AHP in normal ACSF, while the amplitude of sADP was quantified at 1 sec from the last spike of bursts. The local application of DHPG in the soma or proximal dendrite resulted in mADP (Fig. 13A, B, and D), but the magnitude was much smaller compared to that induced by mADP induced by bath application of DHPG shown in Fig. 10. Interestingly, the local application of DHPG in distal dendrite resulted in larger mADP (Fig. 13C and D), indicating that target ion channels underlying mADP generation are distributed more densely in distal dendrites compared to perisomatic region. The DHPG-induced sADP was observed with similar value by local application in soma, proximal dendrite, or distal dendrite (Fig. 13A, B, C, and E). I also analyzed RMP changes, and found that DHPG application to somatic region and proximal dendritic region induced depolarization (Fig. 13A, B, and F), but the local application of DHPG into the distal dendritic region (~250 μm from soma) did not change the membrane potential (Fig. 13C and F).

mGluR5-dependent Ca^{2+} release mediated by cADPR-RyR pathway underlies increased intrinsic excitability

I have recently reported that mGluR5-dependent $I_{Na,P}$ increase is mediated by Ca^{2+}/calmodulin signaling that is activated by intracellular Ca^{2+} release via cADPR/ryanodine receptor (RyR) pathway (22). However, Park et al (39) showed that mGluR-dependent increase in R-type Ca^{2+} currents mediates ADP generation by DHPG. It is possible that different Ca^{2+} sources are involved in regulating different ion channels. To examine this possibility, I analyzed changes in intrinsic excitability under experimental conditions where cADPR/ RyR pathway was blocked. Under these conditions, DHPG-induced RMP depolarization were not significantly affected, but DHPG-induced increase in AP firing as well as DHPG-induced ADP generation were almost completely abolished (Fig. 14A to E), suggesting that these effects are dependent on cADPR/RyR-mediated Ca^{2+} release.

HFS to Shaffer collateral pathway induces Ca^{2+} release which is confined to proximal apical dendrites (22), and the effect of HFS on intrinsic excitability is selective for modulating the timing and precision of AP firing, which is mediated by $I_{Na,P}$ enhancement (Fig. 8 and 9). By contrast, global activation of mGluRs by DHPG induces complex effects on intrinsic excitability (Fig, 10), suggesting that mGluRs target multiple ion channels. I tested the hypothesis that interaction between mGluR5 and target ion channels occurs locally in a restricted region of the neuron. To test this idea, I used Ca^{2+} buffer with different kinetics, BAPTA and EGTA. In the presence of 8 mM

BAPTA, a fast Ca^{2+} buffer in the intracellular solution, DHPG effects on both AP firing and ADP were completely abolished (Fig. 14F and H), while these effects were diminished but not completely abolished in the presence of EGTA, a slow Ca^{2+} buffer (Fig. 14G and H). More powerful effects of BAPTA on inhibiting DHPG-mediated changes compared with EGTA effects suggest that the distance between the Ca^{2+} source and the target ion channels is very close within a nanometer scale so that a slow Ca^{2+} buffer is not sufficient for blocking Ca^{2+} signaling. However, DHPG-induced depolarization still occurred in the presence of BAPTA or EGTA, suggesting that the ion channel mechanisms responsible for DHPG-induced depolarization, possibly activation of TRPC channels (13) or inhibition of leak K^+ channels (49) are not Ca^{2+}-dependent.

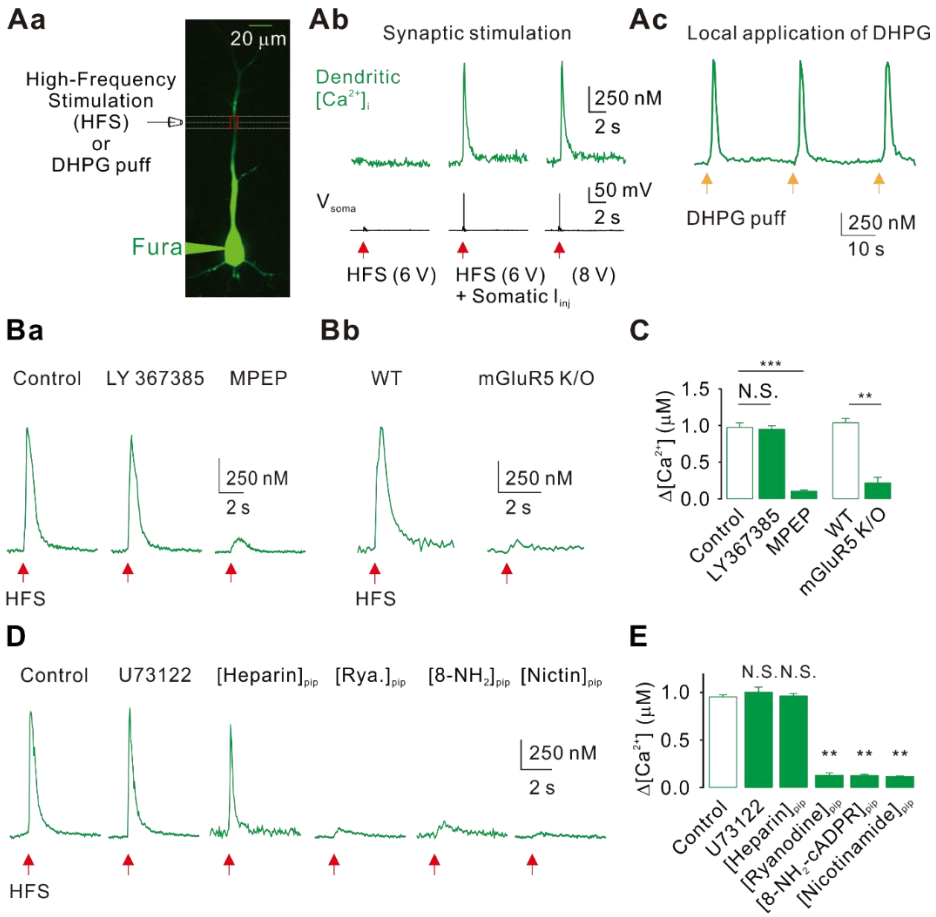

Figure 1. HFS induces mGluR5-dependent dendritic Ca^{2+} release at apical dendrites of CA1-PNs.

Aa, Representative fluorescence image of a CA1-PN filled with 100 μM Fura-2 during whole-cell recording. An extracellular stimulating electrode was placed ~100 μm from the soma and ~50 μm away from the dendrites of interest (red box). *Ab*, Representative $[Ca^{2+}]_i$ transients measured at a dendritic location ~100 μm from the soma in response to subthreshold HFS only, subthreshold

HFS with somatic current injection (I_{inj}; middle), or HFS at suprathreshold intensity that could evoke two or three APs (Bottom; V_{soma}). *Ac*, Representative $[Ca^{2+}]_i$ transients in response to repetitive (every 30 seconds) local applications of DHPG (250 μM, 0.5 sec). Red (*Ab*) or yellow (*Ac*) arrows indicate the time points of corresponding stimulation. *Ba*, $[Ca^{2+}]_i$ increases were not affected by 25 μM LY367385 (middle) but were blocked by 10 μM MPEP (right). *Bb*, $[Ca^{2+}]_i$ transients in response to HFS on CA1-PNs from WT (left) and mGluR5 K/O (right) mice. *C*, Summary of the amplitude of $[Ca^{2+}]_i$ transients under each condition, indicating that HFS at SC synapses cause mGluR5-dependent Ca^{2+} release (Control, n = 10; LY367385, n = 8; MPEP, n = 7; WT, n = 6; mGluR5 K/O, n = 6; Control vs LY367385, $p = 1.0$; Control vs MPEP, $p < 0.0005$; WT vs K/O, $p < 0.01$). *D*, Representative traces for $[Ca^{2+}]_i$ responses to HFS in control and in the presence of U73122 (20 μM, n = 8) in bath solutions, and heparin (1 mg/1 ml, n = 8), ryanodine (100 μM, n = 5), nicotinamide (5 mM, n = 5), and 8-NH_2-cADPR (100 μM, n = 6) in pipette solutions. *E*, Summary of the amplitude of $[Ca^{2+}]_i$ responses under each condition indicates that HFS causes cADPR-dependent Ca^{2+} release from the intracellular store (Control, n = 7; U73122, n = 8; $[Heparin]_{pip}$, n = 8; $[Ryanodine]_{pip}$, n = 5; $[8\text{-}NH_2\text{-}cADPR]_{pip}$, n = 6; $[Nicotinamide]_{pip}$, n = 5; Control vs $[Ryanodine]_{pip}$, $p < 0.01$; Control vs $[8\text{-}NH_2\text{-}cADPR]_{pip}$, $p < 0.01$; Control vs $[Nicotinamide]_{pip}$, $p < 0.01$). Error bars indicate SEM. **$p < 0.01$, ***$p < 0.001$. N.S., not significant.

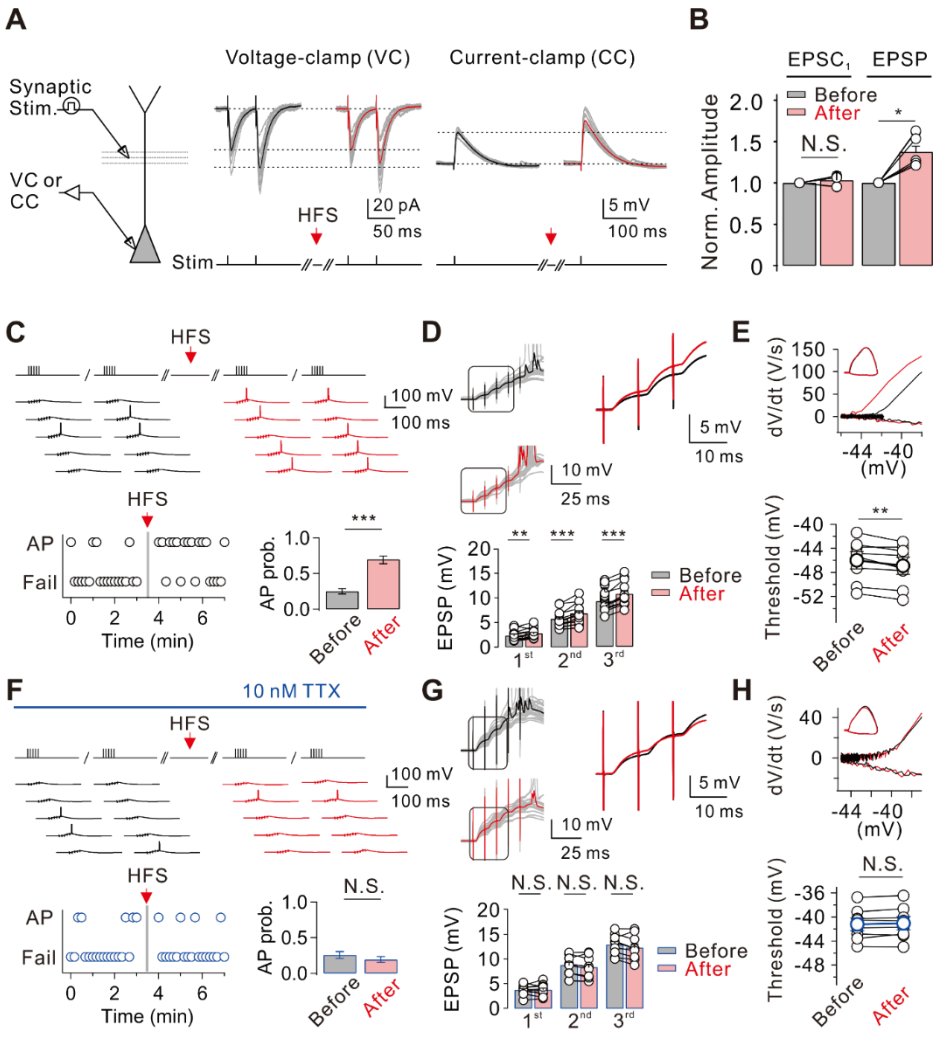

Figure 2. HFS at SC fibers causes Na^+ channel-mediated post-tetanic potentiation of EPSP-spike coupling in CA1-PNs.

A, Left, experimental configuration showing somatic patch-clamp recording in voltage-clamp (VC) or current-clamp (CC) configuration, combined with presynaptic stimulation of the SC. Middle, twelve consecutive traces of EPSCs (grey; 5-s repetition interval) evoked by paired pulse stimulation, are overlaid

with the average EPSC before (left; black) and after (right; red) HFS. Right, twelve consecutive traces of EPSPs (grey; 3 s repetition interval) evoked by a single stimulus, are overlaid with the average EPSP before (left; black) and after (right; red) HFS. *B*, Summary of the peak amplitude of the first EPSCs (n = 5) and EPSPs (n = 6) after HFS (red) normalized to the control amplitude before HFS (grey) suggesting the postsynaptic expression of potentiation. *C,F*, Top, representative traces of somatically measured voltage in response to a short, high-frequency train stimulation (5 stimuli at 100 Hz), repeated every 10-s before (black) and after (red) HFS in control (*C*) and in TTX (10 nM; *F*). Bottom left, whether or not the AP was evoked during a short train was analyzed and plotted against time. Bottom right, summary graph shows the increased probability of AP firing in control (*C*), but no significant difference in TTX (*F*) after HFS. *D,G*, Top left, representative somatic voltage responses (20 samples for each group) to short train stimulation (5 pulses, 100Hz) before (black) and after (red) HFS. Averaged EPSP traces are superimposed on the right. Bottom, summary of the peak amplitude of the first, second, and third EPSPs in the burst exhibiting the potentiation after HFS (n = 12). Note that the potentiation after HFS is occluded in TTX (n = 9; *G*). *E,H*, Top, phase-plane plots of d*V*/d*t* vs corresponding voltage from AP traces before (grey) and after (red) HFS are shown superimposed. Note that the threshold for AP initiation is shifted after HFS in control (n = 8; *E*) but not in TTX (n = 8; *H*), suggesting that HFS at SC-CA1 synapses induces Na^+ channel-mediated increase in dendritic excitability, resulting in decreased threshold value for axosomatic APs. Vertical bars (grey) define the time points of HFS application. Lines connect data points from the

same experiment for clarity. Error bars indicate SEM. *p < 0.05, **p < 0.01, ***p < 0.001. N.S., not significant.

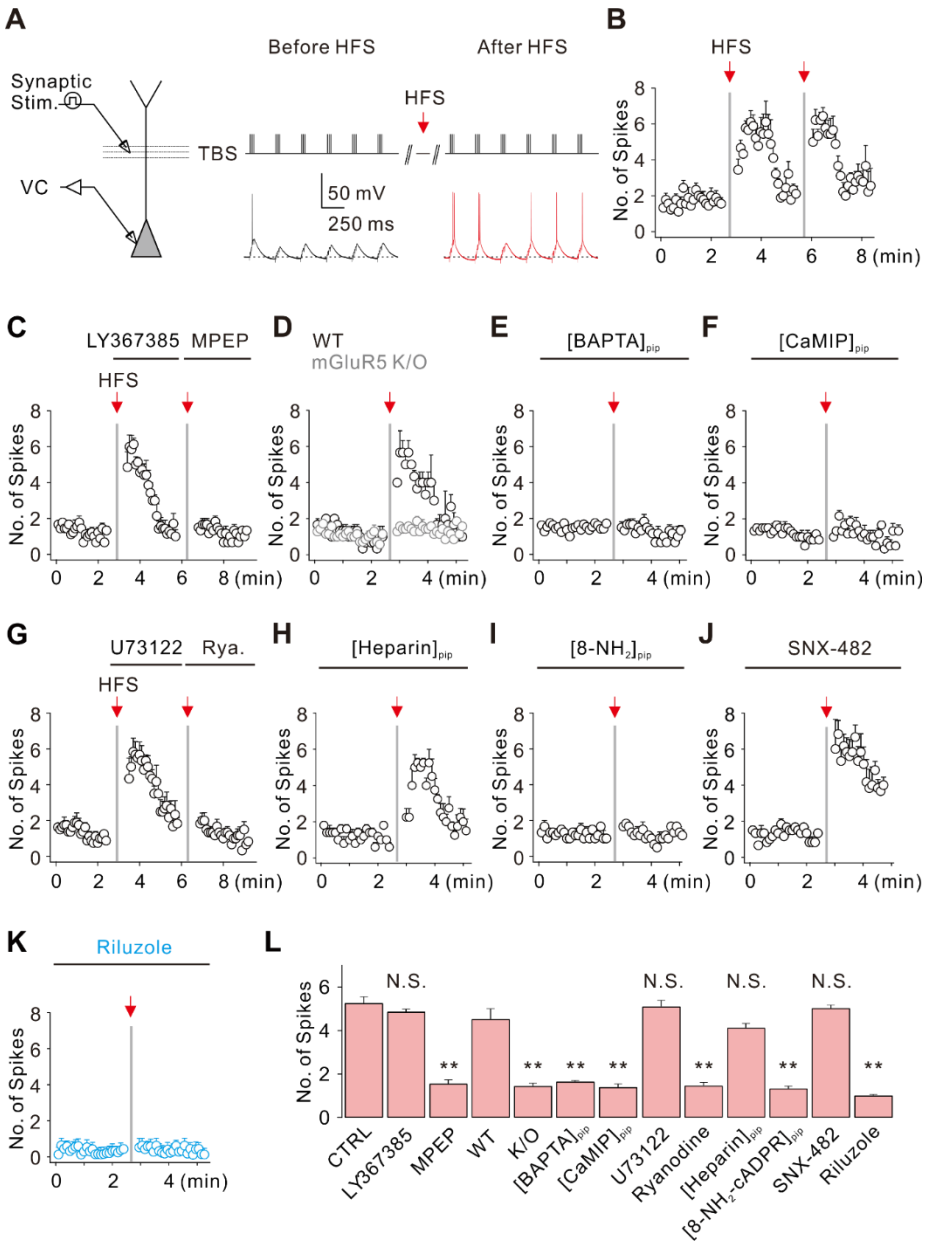

Figure 3. HFS-induced PT-ESP occurs via mGluR5-dependent Ca^{2+} signals.

A, Left, experimental configuration illustrating somatic whole-cell recording

with extracellular stimulation of SC synapses. Right, representative traces of somatically recorded voltages during theta-burst stimulation (TBS; top, 5 synaptic stimulations at 100 Hz repeated 6 times at 4 Hz) before (black) and after (red) HFS. Note that AP firing patterns during TBS were changed after HFS. *B*, Number of spikes evoked by each TBS was counted and plotted against time (n = 9). *C–J*, Summary plots of the mean number of APs evoked by TBS as a function of time under the conditions as indicated (*C*, 25 μM LY367385 and 10 μM MPEP; *D*, WT mice and mGluR5 K/O; *E*, xx 10 mM BAPTA in pipette; *F*, 20 μM CaMIP in pipette; *G*, 20 μM U73122 and 100 μM Ryanodine; *H*, Heparin (1 mg/1 ml) in pipette solutions; *I*, 100 μM 8-NH_2-cADPR in pipette solutions; *J*, 0.5 μM R-type Ca^{2+} channel blocker, SNX-482; *K*, 100 μM Riluzole). *L*, Pooled data of the mean number of APs during TBS obtained for 1 min after HFS in each experimental condition (Control, n = 12; LY367385, n = 6; MPEP, n = 6; WT, n = 4; mGluR5 K/O, n = 8; BAPTA, n = 8; CaMIP, n = 7; U73122, n = 6; Ryanodine, n = 6; $[Heparin]_{pip}$, n = 5; $[8\text{-}NH_2\text{-}cADPR]_{pip}$, n = 6; SNX-482, n = 5; Riluzole, n = 8; Control vs MPEP, $p < 0.01$; WT vs mGluR5 K/O, $p < 0.01$; Control vs $[BAPTA]_{pip}$, $p < 0.01$; Control vs $[CaMIP]_{pip}$, $p < 0.01$; Control vs Ryanodine, $p < 0.01$; Control vs $[8\text{-}NH_2\text{-}cADPR]_{pip}$, $p < 0.01$; Control vs Riluzole, $p < 0.01$), indicating the involvement of mGluR5-dependent Ca^{2+} signaling in HFS-induced PT-ESP. Vertical grey bars indicate the time points of HFS application. Error bars indicate SEM. **$p < 0.01$, not significant.

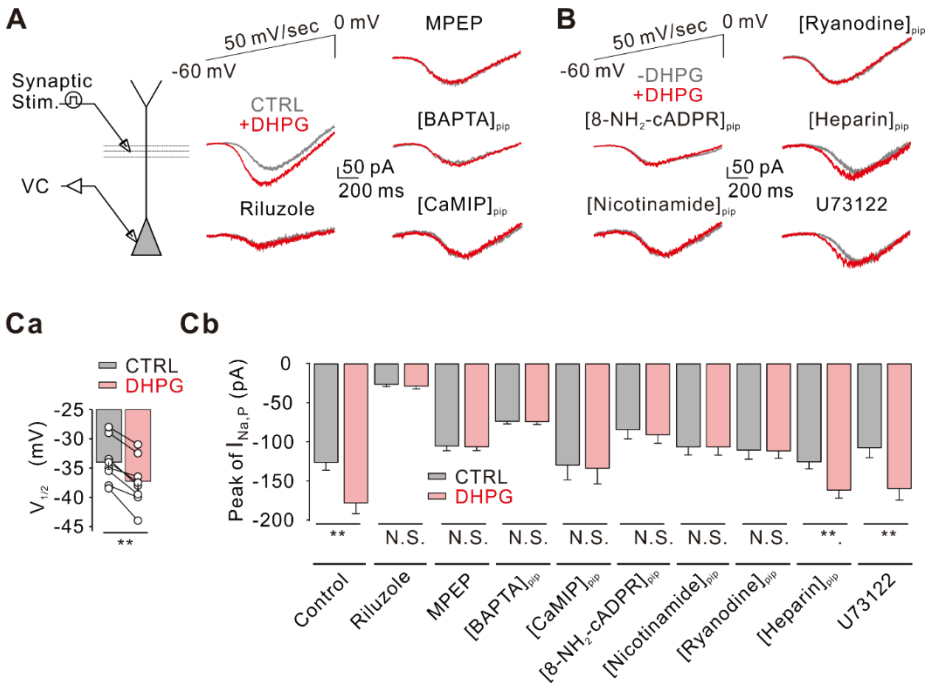

Figure 4. $I_{Na,P}$ is enhanced by mGluR5-induced Ca^{2+} signaling.

A, Left, experimental configuration showing somatic whole-cell recording with extracellular synaptic stimulation of SC synapses. Right, representative traces of somatically recorded whole-cell currents in response to voltage ramp from −60 mV to 0 mV (50 mV/s, top left) before (grey) and after (red) DHPG application in control (left, middle) and in the presence of riluzole (left, bottom), MPEP (right, top), intracellular BAPTA (right, middle), CaMIP in the pipette solutions (right, bottom). *B*, Representative traces of $I_{Na,P}$ in the presence of 8-NH_2-cADPR (100 μM , n = 6), nicotinamide (5 mM, n = 5), ryanodine (100 μM, n = 5), and heparin (1 mg/1 ml, n = 5) in pipette solutions or U73122 (20 μM, n = 5) in bath solutions. *Ca*, Summary data of the effect of DHPG on $V_{1/2}$

(n = 8), suggesting the fast onset of activation of persistent Na^+ channels. *Cb*, Summary of the peak amplitude of $I_{Na,P}$ under different experimental conditions in *A* and *B* (Control, n = 12; Riluzole, n = 14; MPEP, n = 10; BAPTA, n = 6; CaMIP, n = 7; $[8\text{-}NH_2\text{-}cADPR]_{pip}$, n = 6; $[Nicotinamide]_{pip,}$ n = 5; Ryanodine, n = 5; $[Heparin]_{pip}$, n = 5; U73122, n = 5; Control, $p < 0.01$; $[Heparin]_{pip}$, $p < 0.01$; U73122, $p < 0.01$), confirming that the potentiation of $I_{Na,P}$ is dependent on mGluR5-mediated Ca^{2+} signaling. Lines connect data points from the same experiment for clarity. Error bars indicate SEM. **p < 0.01. N.S., not significant.

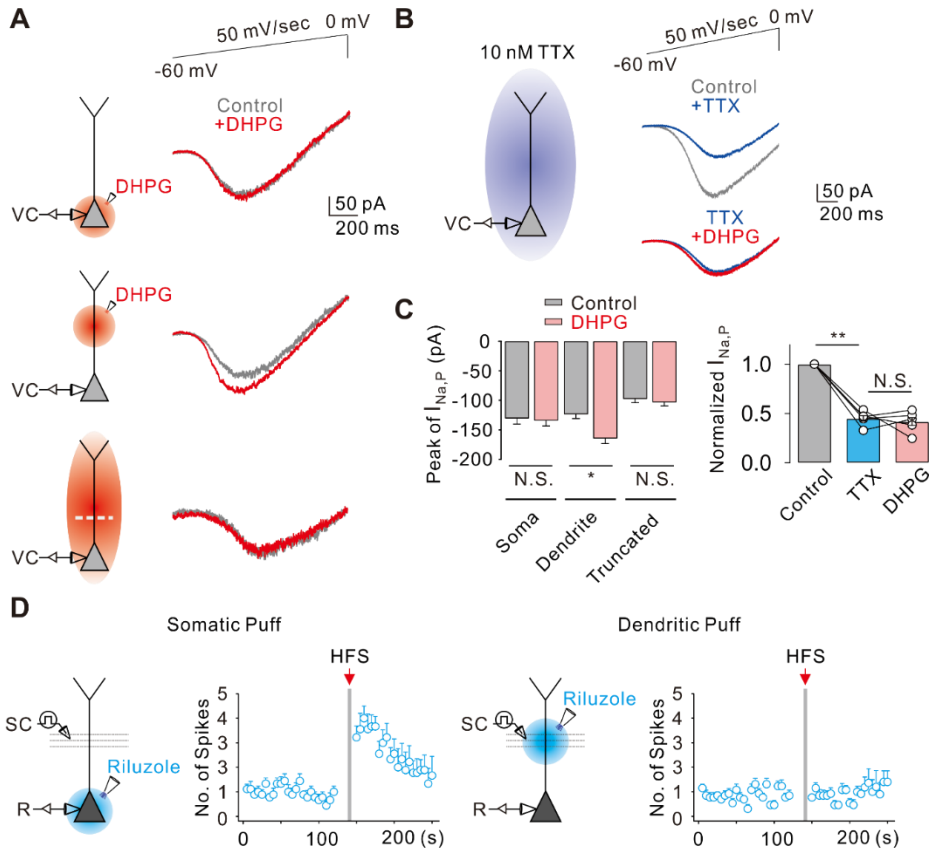

Figure 5. mGluR5-dependent signaling results in enhancement of $I_{Na,P}$ in apical dendrites of CA1-PNs.

A, Left, schematic diagram illustrating the recording configuration. DHPG is applied either by bath perfusion (bottom) or by local application to the soma (top) or the proximal dendrite (center) with a pressure application system. Right, representative traces of somatically recorded whole-cell currents in response to voltage ramp from −60 mV to 0 mV (50 mV/s) before (grey) and after (red) DHPG application. Note that dendrotomy of the entire apical dendrite of CA1-

PNs (bottom) occludes mGluR5-dependent increase of $I_{Na,P}$. *B*, Left, experimental configuration showing the voltage-clamp recording with bath application of 10 nM TTX. Right, representative traces of somatically recorded $I_{Na,P}$ in control and in the presence of 10 nM TTX, with or without local application of DHPG (bottom). *Ca*, Pooled data of the peak amplitude of $I_{Na,P}$ under different experimental conditions in *A*. *Cb*, Pooled data of the normalized amplitude of $I_{Na,P}$ in each condition in *B*. *D*, Experimental configuration showing somatic recording with TBS/HFS stimulation of the SC pathway, combined with local somatic (left) or dendritic (right) application of 50 μM riluzole. Right, summary plots of average number of APs evoked by TBS as a function of time in each condition. Vertical grey bars define the time points of HFS application. Error bars indicate SEM. *$p < 0.05$; **$p < 0.01$. N.S., not significant.

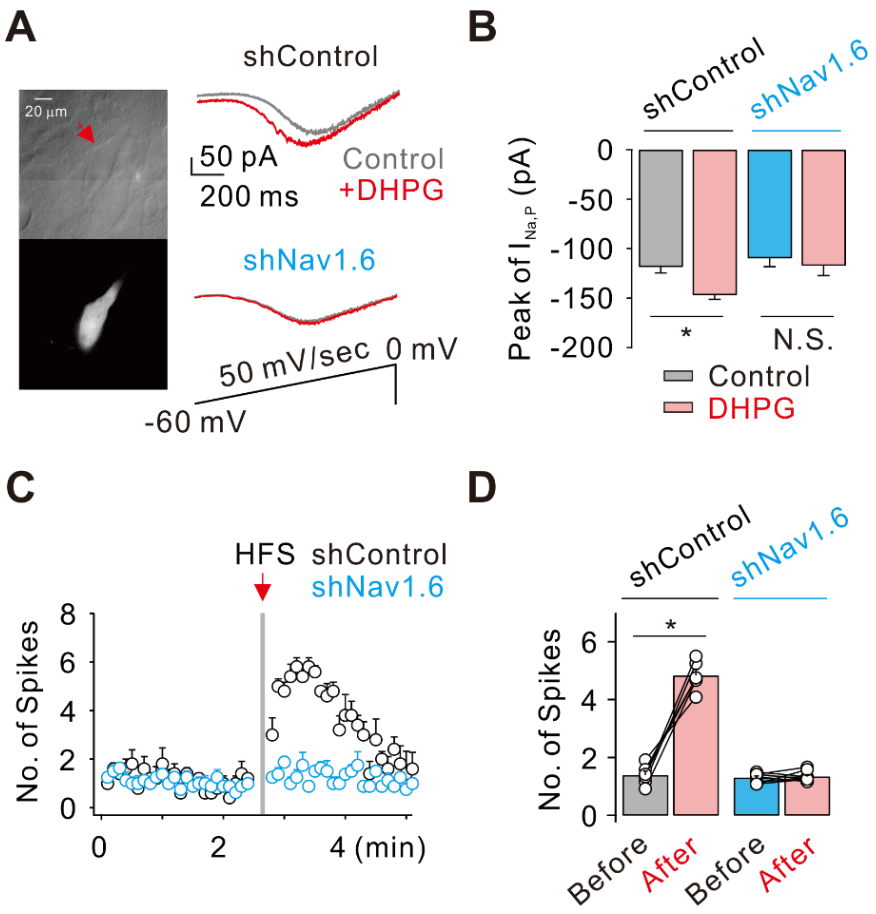

Figure 6. Knockdown of Nav1.6 abolishes HFS-induced PT-ESP.

A, Representative infrared differential interference contrast video image (top) and fluorescence image (bottom) of a CA1-PN transfected with scrambled shRNA. *B*, Left, representative traces before (grey) and after (red) DHPG application recorded from hippocampal neurons transfected with scrambled shRNA (shCTRL, top) or Nav1.6 shRNA (shNav1.6, middle). Bottom panel indicates voltage ramp from −60 mV to 0 mV (50 mV/s). Right, summary bar graphs of the averaged peak amplitude of $I_{Na,P}$ in each condition (shCTRL, n = 6; shNav1.6, n = 5). *C*, Plot of the number of APs evoked by TBS in neurons

transfected with shCTRL or shNav1.6. *D*, Bar graphs show the mean number of APs during TBS obtained for 1 min before and after HFS in each condition before (shCTRL, grey; shNav1.6, blue) and after (red) HFS (shCTRL, n = 8; shNav1.6, n = 6). Vertical red bars define the time points of HFS application. Lines connect data points from the same experiment. Error bars indicate SEM. *p < 0.05; **p < 0.01. N.S., not significant.

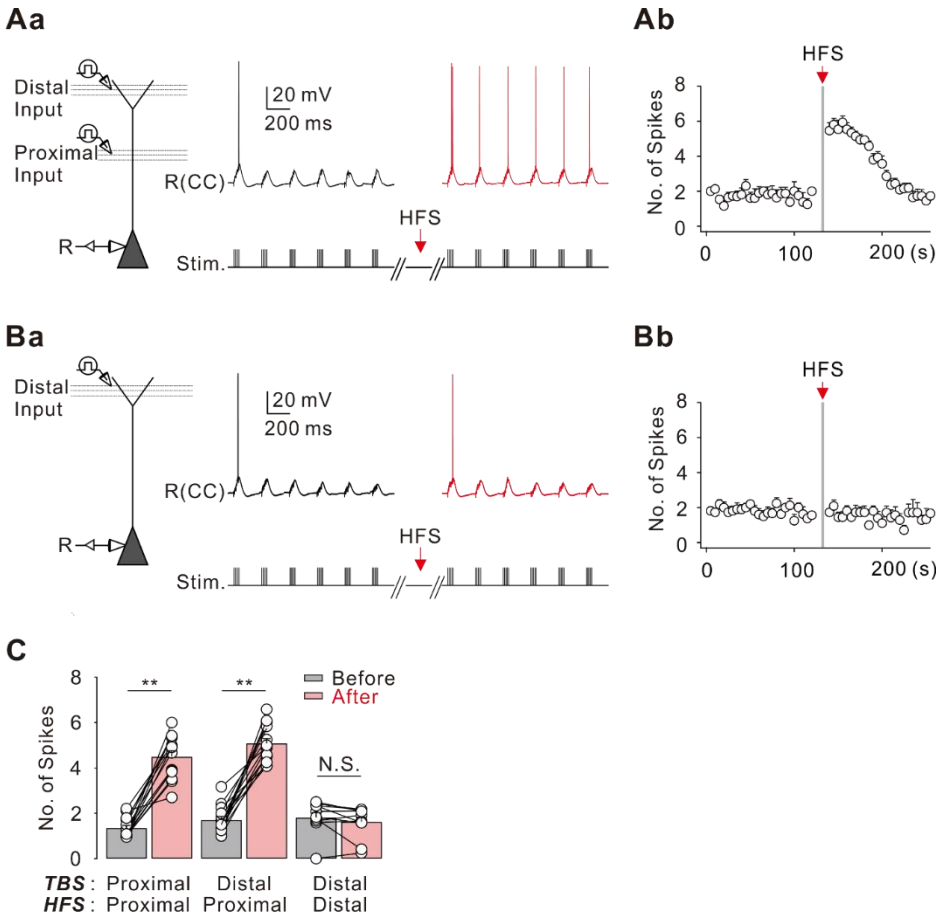

Figure 7. PP inputs to CA1-PNs are potentiated by HFS of SC but not PP inputs.

Aa, Experimental configuration showing somatic current-clamp recording (CC) with extracellular electrodes positioned to stimulate PP and SC inputs. Representative traces of somatically recorded voltages in response to TBS at distal synapses (> 250 μm; approximately corresponding to the stratum lacunosum-moleculare) before (black) and after (red) HFS of the SC (~100 μm).

Ab, The number of somatic APs evoked by TBS at distal synapses before and after HFS against time (n = 10). *Ba*, Experimental configuration and representative traces of summated EPSP recorded from the soma in response to TBS at the distal dendrites before (black) and after (red) HFS, which was applied to the same region. *Bb*, The number of APs evoked by TBS at proximal synapses before and after HFS against time (n = 7). *C*, Bar graphs summarize the number of APs obtained for 1 min before and after HFS in each condition (Left, n = 14; Middle, n = 15; Right, n = 11), indicating that HFS at proximal—but not at distal synapses—can induce a significant short-term potentiation at both proximal and distal synapses. Vertical red bars define the time points of HFS application. Error bars indicate SEM. **p < 0.01. N.S., not significant.

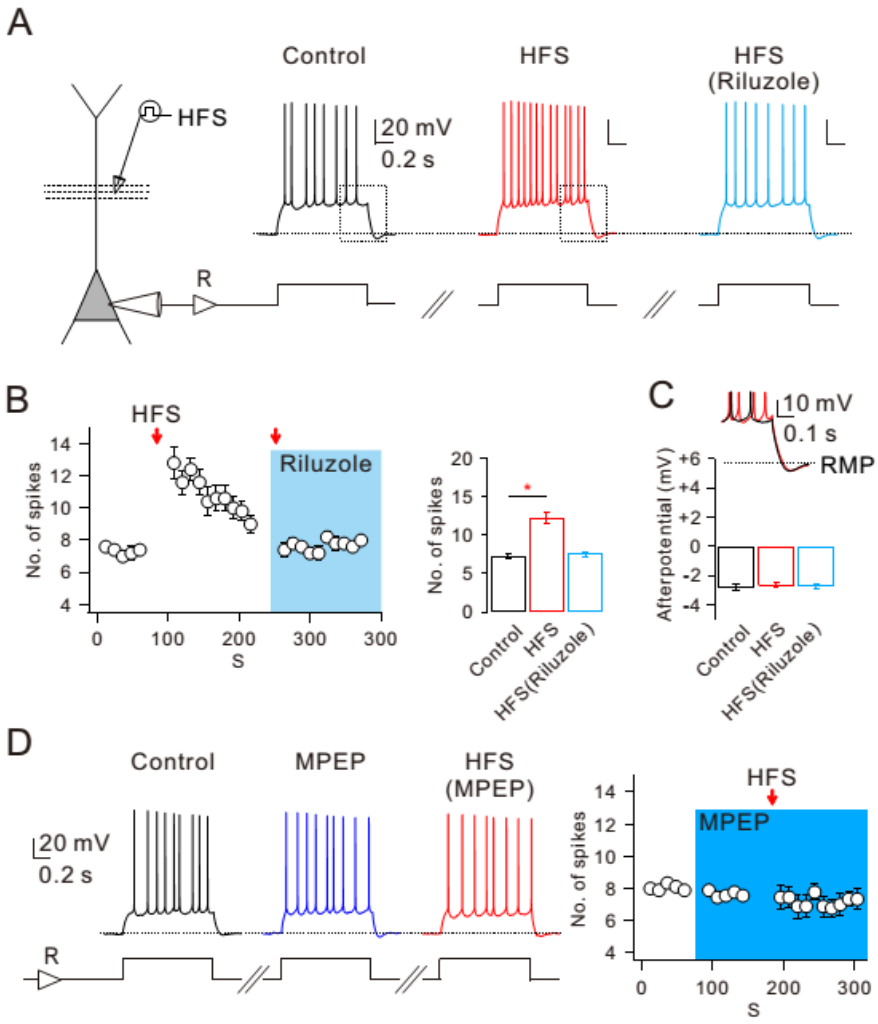

Figure 8. mGluR5-dependent increased CA1 neuronal excitability is mediated by enhancement of $I_{Na,P}$

A, left, schematic diagram illustrating the recording configuration showing somatic current-clamp recording (CC) with extracellular electrodes positioned to stimulate SC inputs. Right, representative traces demonstrated HFS-increased number of spikes in response to square current injections before HFS (black), after HFS (red), and after HFS in riluzole (blue, 10 μM). *B,* left, number

of spikes evoked by somatic current injections was counted and plotted against time (n = 5). Right, pooled data of the mean number of spikes during somatic current injection obtained for first 1 min in each condition (n = 5, control vs HFS, *P < 0.05). *C*, top, inset shows superimposed view corresponding to the box shown in *A*. Bottom, pooled data of the afterpotential following square currents injections in different conditions (n = 5). *D*, left, representative traces demonstrate the effects of MPEP (10 μM) on HFS-induced changes of number of spikes. Right, summary plots of the mean number of spikes evoked by somatic current injections as a function of time (n = 9).

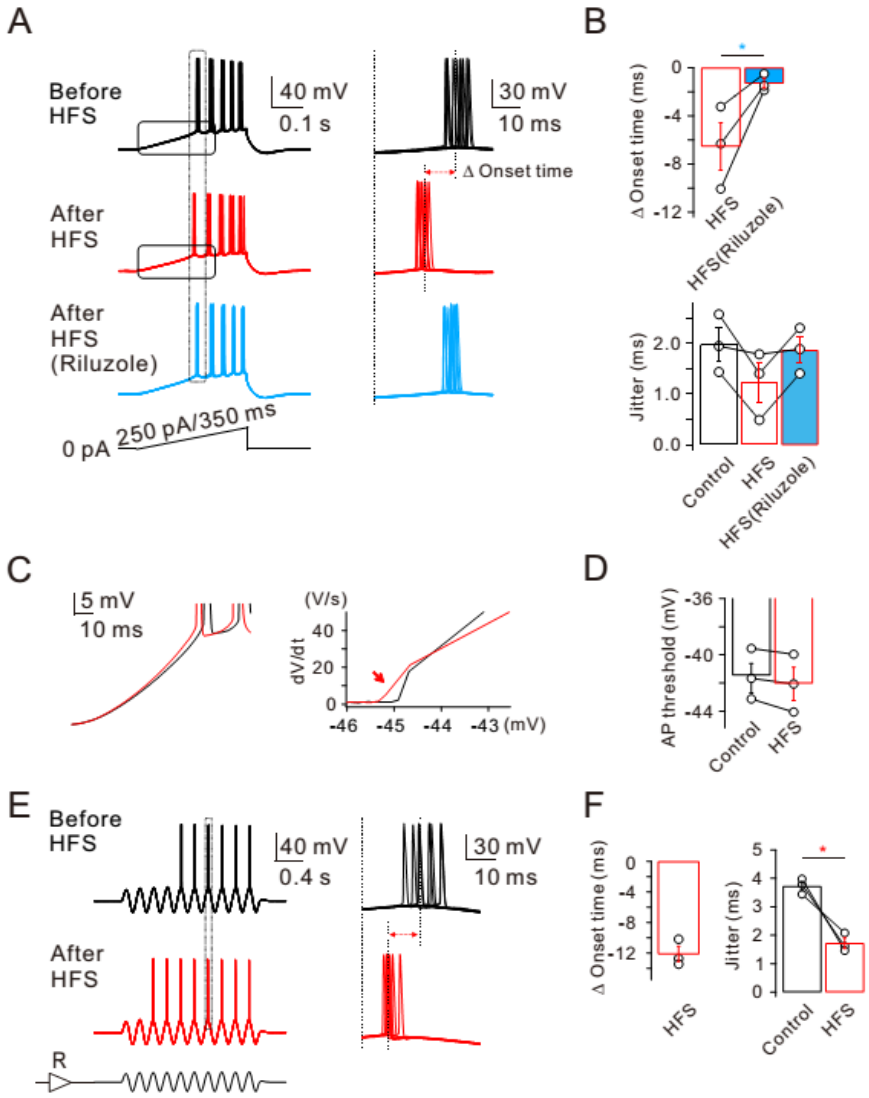

Figure 9. HFS-induced decrease of spike onset timing and jitter

A, left, representative traces in response to slow current ramp (250 pA/350 ms) injections before (black), after (red), and after in riluzole (bottom, blue). Right, representative traces demonstrate HFS-decreased spike timing onset and jitter are reversed by riluzole. *B,* pooled data summarizes the effects of HFS and

subsequent addition of riluzole on spike onset timing and jitter (Δ onset time, *n* = 3, HFS vs HFS (Riluzole), **P* < 0.05). *C*, left, averaged voltage traces from the traces shown in (*A*) before (black) and after (red) HFS are superimposed. Right, phase-plane plots of d*V*/d*t* vs corresponding voltage from the traces shown in (left, *C*) before (black) and after (red) HFS are shown superimposed. Note that the threshold for AP initiation is shifted after HFS in control (red arrow in *C*, *n* = 3; *D*). *E*, left, representative traces in response to sine wave current with theta frequency (5 Hz) via somatic pipette before (black) and after HFS (red). *F*, pooled data summarizes the effects of HFS in response to sine wave currents injection on spike onset timing and jitter (jitter, *n* = 3, control vs HFS, **P* < 0.05)

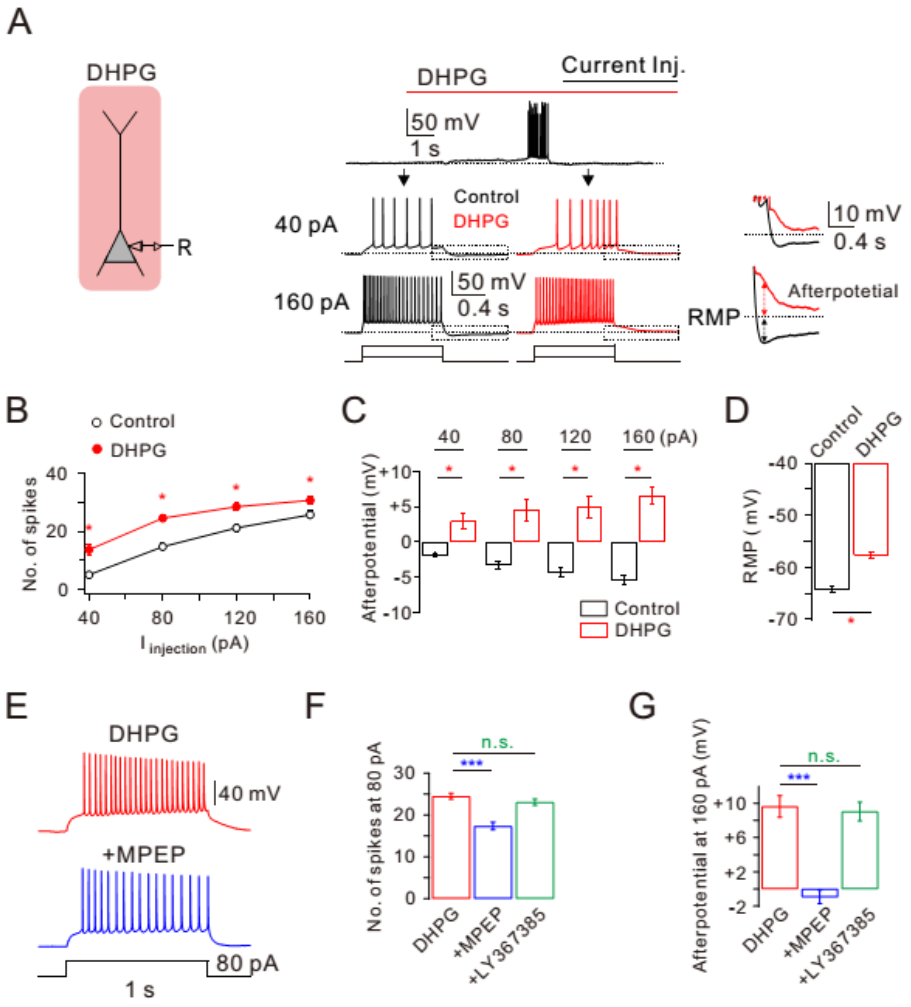

Figure 10. Bath applications of DHPG stimulates mGluR5 to increase hippocampal CA1 neuron excitability.

A, left, a schematic drawing of experimental condition demonstrates a neuron being recorded with bath applications of DHPG. Right, representative traces demonstrate DHPG-induced depolarization of membrane potential (upper trace) and changes in AP firing frequency and afterpotential in response to square pulse injections (40 pA, 160 pA, lower traces). Note that afterpotentials

following 2 different magnitudes of current injections. *B*, FI curve summarizes the effects of DHPG on AP firing frequency in response to square current injections (n = 16, control vs DHPG, *P < 0.05). *C*, bar graphs summarize the effects of DHPG on afterpotentials following 4 different square current injections (n = 5, control vs DHPG, *P < 0.05). *D*, bar graphs summarize the effects of DHPG on resting membrane potentials (n = 5, control vs DHPG, *P < 0.05). E, Representative traces demonstrate the effects of MPEP on DHPG-induced changes of AP firing frequency and afterpotentials. *F*, pooled data of the mean number of spikes following 80 pA square pulse injections in each condition (DHPG, n = 14; MPEP, n = 14; LY367385, n = 16, DHPG vs MPEP, ***P < 0.001; DHPG vs LY367385, n.s., P > 0.05). *G*, bar graphs summarize the effects of DHPG and subsequent addition of MPEP or LY367385 on afterpotentials following 160 pA square pulse injections (DHPG, n = 7; MPEP, n = 10; LY367385, n = 7; DHPG vs MPEP, ***P < 0.001; DHPG vs LY367385, n.s., P > 0.05).

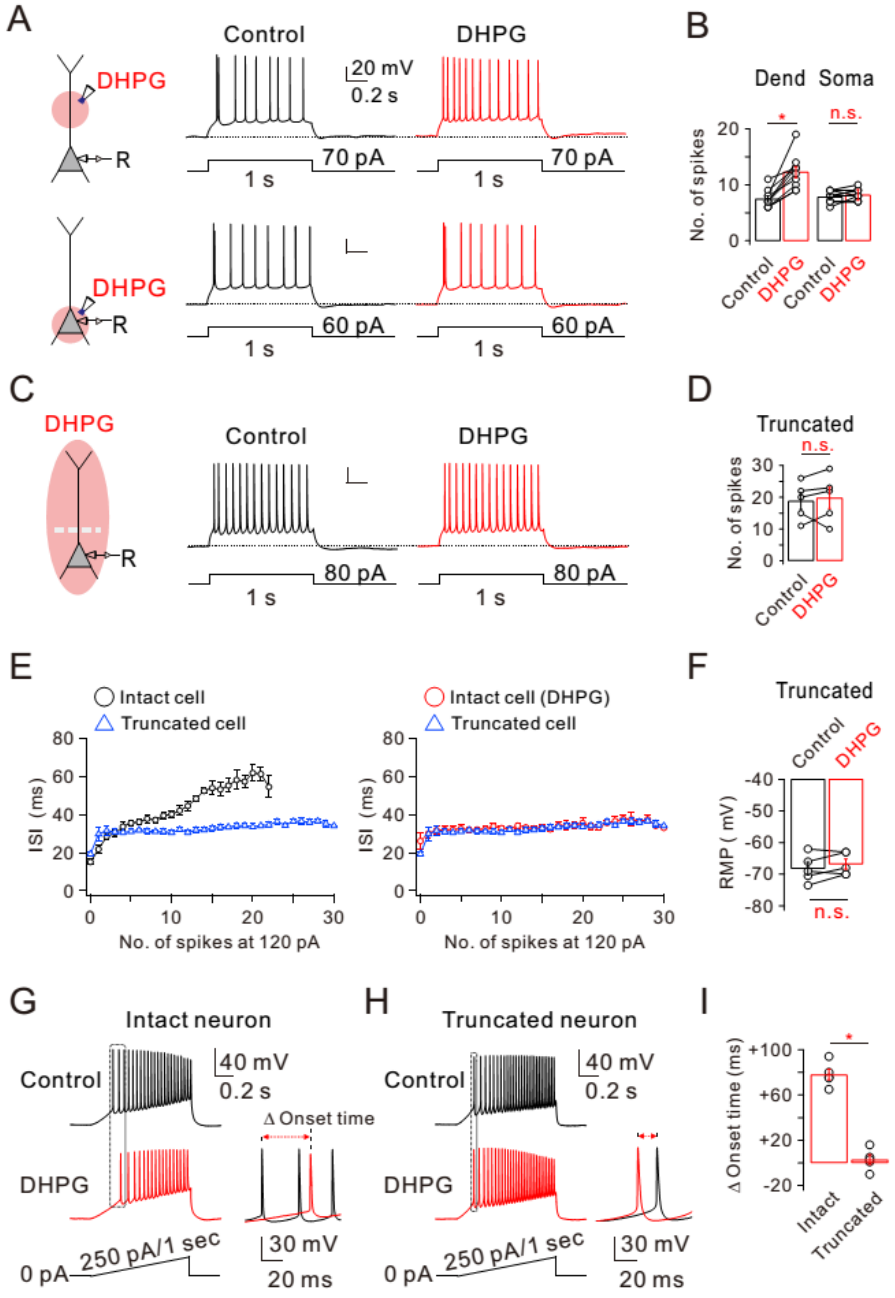

Figure 11. Dendritic $I_{Na,P}$ is selectively modulated by DHPG on AP firing in CA1 neuron.

A and *C* left, a schematic drawing of experimental condition demonstrates a neuron being recorded with dendritic or somatic local applications of DHPG (250 μM). *A*, right, representative traces demonstrate the effects of local application of DHPG on AP firing frequency and afterpotentials. *B*, pooled data of the mean number of spikes during somatic current injection in each condition (Dend, $n = 10$; Soma, $n = 11$; Dend, Control vs DHPG, *P < 0.05; Soma, Control vs DHPG, n.s., $P > 0.05$). *C*, right, representative traces demonstrate the effects of application of DHPG on AP firing frequency and afterpotentials in truncated CA1-PNs. *D*, pooled data of the mean number of spikes during somatic current injection ($n = 5$, n.s., $P > 0.05$). *E*, inter-spike interval (ISI) was plotted against spiking number in each condition (intact cells, n = 5; truncated cells , n = 5). *F*, bar graphs summarize the effects of DHPG on resting membrane potentials in truncated cells ($n = 5$, n.s., $P > 0.05$). *G and H*, left, representative traces in response to slow current ramp (250 pA/1 sec) injections before (black) and after DHPG (red) in intact CA1-PNs or truncated CA1-PNs. *I*, pooled data summarizes the effects of DHPG on spike onset timing ($n = 5$, $*P < 0.05$).

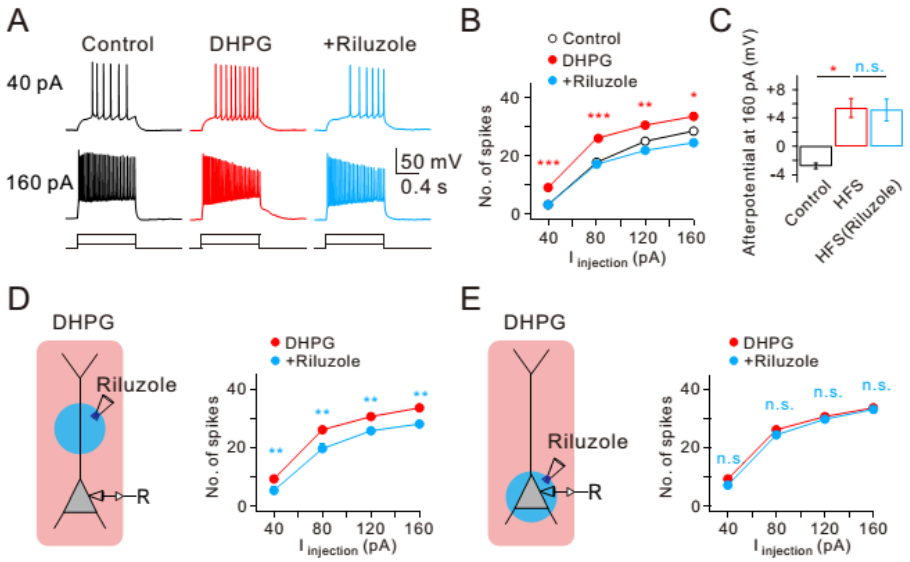

Figure 12. DHPG-induced increase of intrinsic excitability requires dendritic persistent Na^+ currents.

A, representative traces demonstrate the effects of DHPG and subsequent addition of riluzole of AP firing frequency and afterpotentials at current injections of 40 pA and 160 pA. *B*, FI curve summarizes the effects of DHPG and subsequent addition of riluzole on AP firing frequency in response to square pulse injections. (n = 8, control vs. DHPG, *P < 0.05, **P < 0.01, ***P < 0.001). *C*, Bar graphs summarize the effects of DHPG and subsequent addition of riluzole on afterpotentials following 160 pA square pulse injections. (n = 8, control vs. DHPG, *P < 0.05, n.s., P > 0.05) *D* and *E*, left, a schematic drawing of experimental condition demonstrates a neuron being recorded with somatic local applications of riluzole. *D*, right, FI curve summarizes the effects of DHPG and subsequent dendritic local addition of riluzole on AP firing

frequency in response to square pulse injections (n = 8, DHPG vs riluzole, **P < 0.01). *E*, right, FI curve summarizes the effects of DHPG and subsequent somatic local addition of riluzole on AP firing frequency in response to square pulse injections (n = 8, DHPG vs. riluzole, n.s., P > 0.05).

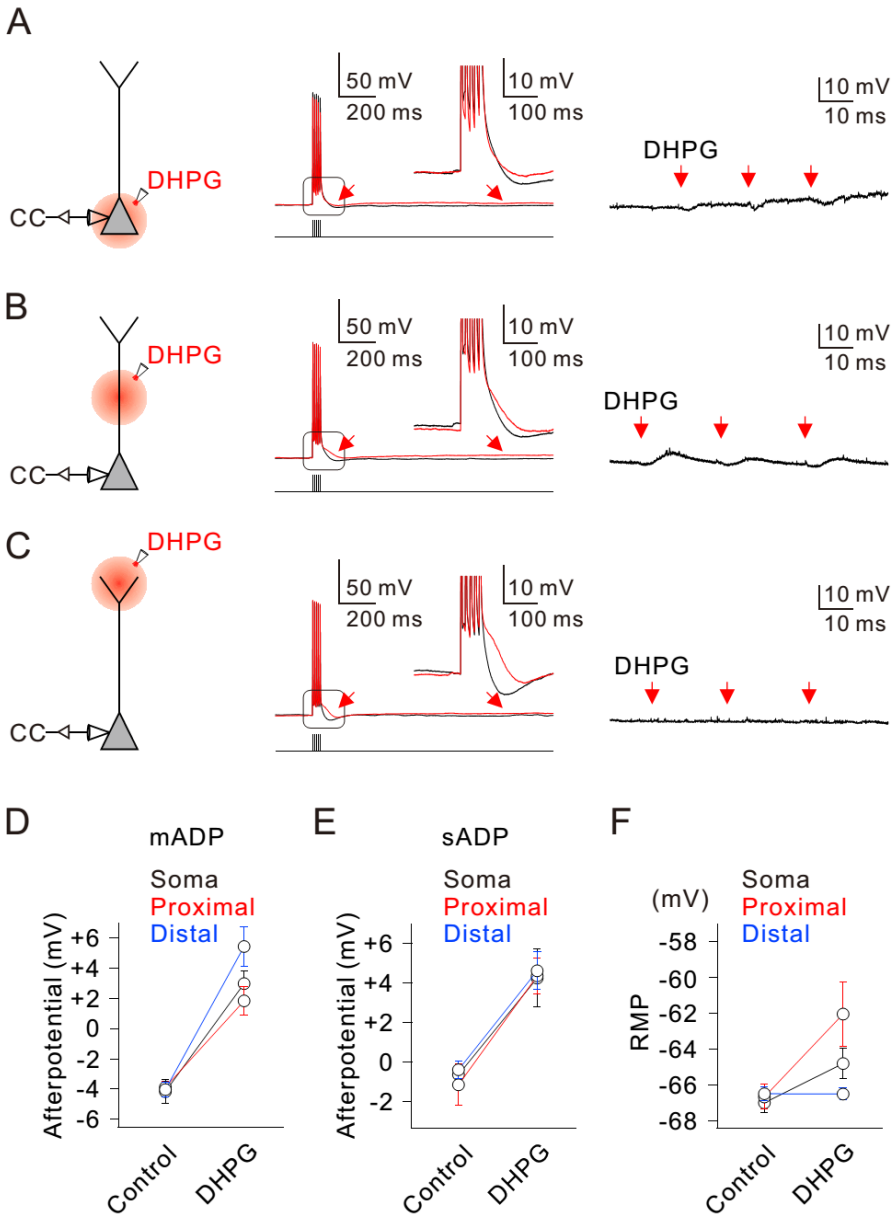

Figure 13. The afterpotential induced by DHPG is differentially regulated along the somatodendritic axis.

A~*C*, left, schematic diagram illustrating the recording configuration. DHPG is applied by local application to soma (*A*), proximal dendrite (*B*), or distal dendrite (*C*) with a pressure application system. *A*~*C*, middle, response to five brief current injections (1 nA, 3 ms, 100 Hz each) to evoke a burst of action potentials in control (black) or DHPG (red). First arrow indicates mADP and second arrow indicates sADP. Inset shows an expanded view corresponding to the box shown in the voltage traces. *A*~*C,* representative traces demonstrate DHPG induced depolarization of membrane potential. Red arrows indicate the time points of corresponding local application of DHPG. *D*~*F*, pooled data of the effects of DHPG on mADP (*D*), sADP (*E*), and resting membrane potentials (*F*) in each condition (soma, n = 5, black; proximal, n = 3, red; distal, n = 6, blue).

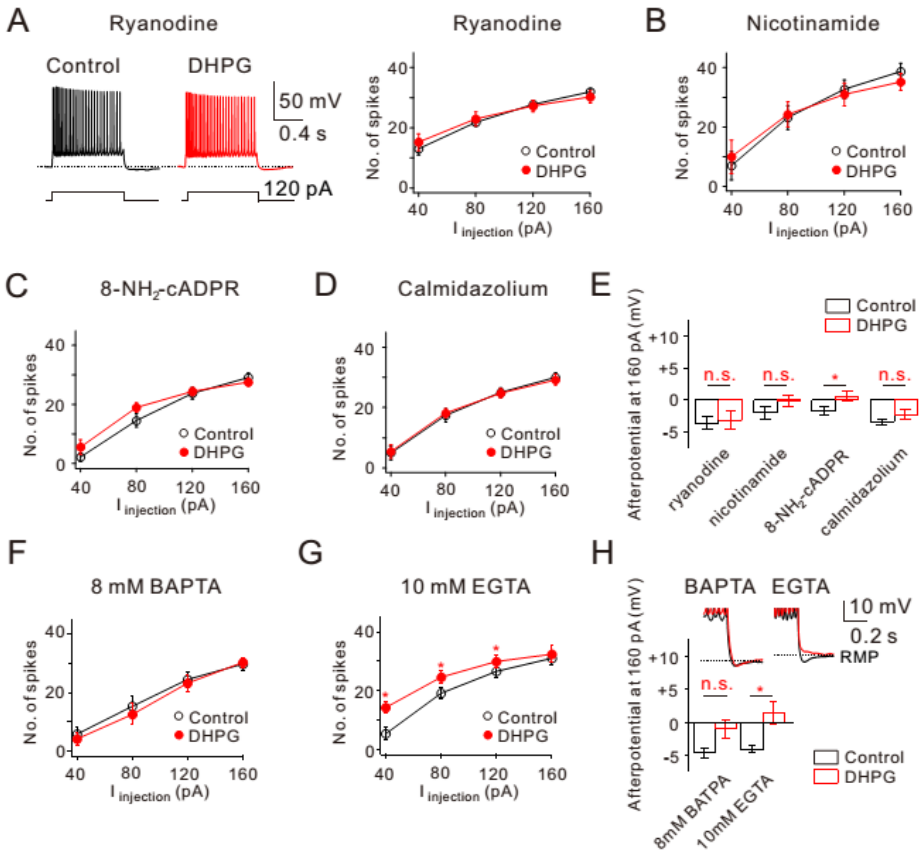

Figure 14. DHPG-induced increase of intrinsic excitability requires intracellular Ca^{2+}

A, left, representative traces demonstrate the effects of DHPG on AP firing frequency and afterpotentials at 120 pA current injections when ryanodine (20 μM) was added to the pipette solutions. Right, FI curve summarizes the effects of DHPG on AP firing frequency in response to square pulse injections (n = 4). *B–D*, summary plots of the FI curve under the conditions indicated (*B*, n = 4, 5 mM nicotinamide; *C*, n = 5, 100 μM 8-NH_2-cADPR; *D*, n = 5, 3 μM calmidazolium). *E*, bar graphs summarize the effects of DHPG on

afterpotentials following 160 pA square current injections under different conditions indicated (n.s., $P > 0.05$, $*P < 0.05$). *F* and *G*, summary plots of the FI curve under the conditions indicated (*F*, n = 8; *G*, n = 11). *H*, bar graphs summarize the effects of DHPG on afterpotentials following 160 pA square current injections under different conditions indicated (8 mM BAPTA, n = 8, n.s., $P > 0.05$; 10 mM EGTA, n = 11, $*P < 0.05$). Note that DHPG-induced increase of after potential is abolished when 8 mM BAPTA was added to the pipette solutions.

Discussion

Traditionally, activity-dependent plasticity in neural circuits has been assumed to be synaptic plasticity. However, increasing evidence supports that neuronal intrinsic plasticity may also be modulated by activity-dependent manner (2, 50). In layer 5 pyramidal neurons, a potentiation of intrinsic neuronal excitability was found. Also, a localized decrease in AP threshold and Na^+ channel activation voltage have been reported with LTP induction (2). These intrinsic plasticity occurs during behavioral learning tasks in adult animals as well as in developing brain (51). In the present study, adding another evidence about this type of plasticity, I demonstrate here an mGluR5 dependent post-tetanic modulation of dendritic excitability. This intrinsic potentiation does not require NMDA and $GABA_A$ receptor activation but is directly induced by mGluR5 dependent pathway and requires localized activation of Ca^{2+} signaling pathway. The activation of mGluR5 leads to increase of firing rate and consequently improve spike-timing precision that is accompanied by decreasing the variability of onset timing. Moreover, I demonstrate that a short period of tetanic stimulations of the SC pathway activates postsynaptic mGluR5-signaling cascade at the synaptic site, which gives rise to an enhancement of dendritic persistent sodium current, thereby increasing the safety factor for spike initiation in the hippocampal CA1-PN dendrites. The upregulation of dendritic $I_{Na,P}$ also enhances the efficacy of distal synaptic inputs, suggesting new evidence for SC inputs as an instructive signal for potentiation of distal inputs. This post-tetanic EPSP-spike potentiation is an unreported form of

short-term plasticity rule, providing a novel insight for understanding the dynamics of hippocampal network operations. Also, mGluR5-induced changes in intrinsic excitability of CA1-PNs may have implications for our understanding of hippocampal memory processing.

PT-ESP, a novel form of short-term plasticity

Tetanic stimulations to synapses are well-known to induce potentiation of synaptic strength. Generally, it is referred to as post-tetanic potentiation (PTP) when the potentiation lasts for several minutes and long-term potentiation (LTP) when the potentiation lasts for more than an hour. PTP has been suggested to play important roles in information processing and working memory (52), whereas LTP is known as a cellular mechanism for storing information (53). In the present study, I demonstrate a cellular plasticity form of PTP driven by HFS for a short duration (0.5 s) to the proximal dendrites, which is distinct from synaptic PTP or LTP. After tetanic induction, dendritic $I_{Na,P}$ at the stimulation sites is increased, leading to potentiation of the EPSPs and facilitation of AP generation for a short duration.

Another feature of PT-ESP is that the increased dendritic $I_{Na,P}$ induced by HFS at the proximal dendrites has a potentiating effect for the EPSPs generated at the distal dendrites (Fig. 2). Pathway interactions between proximal SC inputs and distal PP inputs in CA1-PNs have received much attention in recent studies. When two inputs are paired at a precise interval,

stimulation of distal PP inputs induces LTP at proximal SC synapses (54), suggesting an instructive role of PP inputs. On the other hand, Jarsky et al. (55) showed a gating function of proximal SC inputs when it came slightly after PP inputs. Similarly, Takahashi and Magee (56) reported a drastic change in output mode and an increase in input efficacy of PP input to CA1 by the occurrence of highly correlated SC inputs. In the present study, E-S potentiation of distal inputs after HFS to proximal inputs is also considered to represent a gating function of proximal inputs, but there are several distinctions compared with the previous studies. Opening of gate presented in my study is an intrinsic mechanism and does not require highly correlated interactions between distinct pathways.

In the present study, I applied HFS in the presence of AP5 to exclude the possible contamination of NMDA receptor-dependent mechanisms and investigated mGluR-mediated effects. However, in physiological conditions, it may be possible that NMDA receptor-dependent changes, such as synaptic LTP or intrinsic plasticity (16), are activated together with mGluRs, leading to the synergistic effects. Alternatively, E-S potentiation of both proximal and distal inputs to CA1-PNs in time scale of minutes (< 2 min, Fig. 3) induced by short HFS may act as a metaplastic mechanism to lower threshold for activating NMDA-dependent mechanisms. The increase in AP firing during PT-ESP might help to induce LTP at PP synapses in response to the stimulation, which otherwise not sufficient to induce LTP of the PP synapses in CA1-PNs (4, 57).

Remarkably, a previous in vivo study (26) has shown that single-cell

manipulation of intrinsic excitability of hippocampal CA1-PNs during spatial navigation can non-synaptically and reversibly turns a previously silent cell (without spatially tuned firing) into a place cell (with spatially tuned firing in a defined location of the animal), reflecting that intrinsic excitability is a more important determinant of the firing field rather than the strength of synaptic inputs. The same lab recently reported the study in which the somatic membrane potential of place cells was continuously monitored during exploration of both novel and familiar virtual environments, revealing that the emergence of new place fields does not require sustained depolarization, and that CA1-PNs that later become place cells showed a lower AP threshold and a greater likelihood of firing bursts of APs (27, 29)These results imply the importance of firing ability of CA1-PNs in functioning as place cells. However, the conditions whereby firing ability is modulated, are not well known. Given that PT-ESP can be evoked by physiologically plausible stimulation at CA3-CA1 synapses and involves a reduced AP threshold and increased AP firing rates, our results may have important implications for the role of dendritic $I_{Na,P}$ in mediating place field formation.

Activity-dependent regulation of dendritic $I_{Na,P}$

Persistent sodium currents are present throughout the central nervous system, and they play an important role in neuronal excitability (19). Despite its small magnitude compared to fast Na^+ currents (< 1%), $I_{Na,P}$ has distinct functional significance because of the low activation threshold (~10 mV negative to that of fast Na^+ currents) and non-inactivating property (19). $I_{Na,P}$ in CA1-PNs

contributes to afterdepolarization and associated bursting (42), regulation of spike timing (58), and amplification of EPSPs (59). Recently, Nav1.7-mediated $I_{Na,P}$ in hypothalamic neurons reported to prolong EPSPs, playing an important role in synaptic integration mechanism (60). I found that HFS-induced $I_{Na,P}$ enhancement causes the increase in EPSP amplitude (Fig. 2), but time course of EPSP decay was not significantly affected after HFS. Considering that synaptic integration is the process to which the balance between inward and outward currents, membrane potentials, and input resistance contribute in a complex way, the role of $I_{Na,P}$ in synaptic integration can be different in different type of neurons or in different inputs. Additional studies will be required to understand the mechanisms involved in different roles of $I_{Na,P}$ in synaptic integration.

The subcellular localization of ion channels may have a great impact on functional significance of ion channels in the regulation of neuronal excitability and synaptic integration. Since the focal application of the blockers to the somatic region—but not to the distal dendrites—had effects (42, 59), it was suggested that these functions are attributable to proximal $I_{Na,P}$ localized near the soma. Although the presence of dendritic $I_{Na,P}$ was suggested earlier (19), the role of dendritic $I_{Na,P}$ has remained unclear. Differential localization of Nav1.7 at specific neuronal compartments such as subsets of dendritic branches has been suggested to underlie input-specific processing of EPSPs in hypothalamic neurons (60). I provide evidence that mGluR5 signaling activated by HFS to SC pathway selectively regulates $I_{Na,P}$ in the proximal apical

dendrites of CA1-PNs to cause the enhancement of EPSPs, leading to PT-ESP. Using voltage-clamp experiments for direct recording of $I_{Na,P}$, I demonstrated that focal application of DHPG to dendritic regions—not to perisomatic region—induces an increase in $I_{Na,P}$ (Fig. 5). These results suggest a differential modulation of dendritic $I_{Na,P}$ and perisomatic $I_{Na,P}$ and a specific coupling between mGluR5 and dendritic $I_{Na,P}$. Given that $I_{Na,P}$ can be modulated by various signaling pathways (61, 62), many questions about how $I_{Na,P}$ modulation can influence dendritic excitability and synaptic integration remain to be addressed.

The specific coupling between mGluR5 and dendritic $I_{Na,P}$ leads to the question whether isoform-specific regulation underlies this specificity. Previously, a quantitative EM immunolocalization study has shown the presence of Nav1.6 in the CA1-PN dendrites with a gradual decrease in density along the proximodistal axis (17). Therefore, I anticipated that Nav1.6 could be a major isoform responsible for mGluR5 and dendritic $I_{Na,P}$ coupling. In addition, other Na^+ channel isoforms were not detected in the CA1-PN dendrites, Nav1.6 was suggested as a key substrate controlling dendritic excitability but without direct evidence. I found that dendritic Nav1.6 is a target for mGluR5-induced potentiation of $I_{Na,P}$ (Fig. 5). The result that $I_{Na,P}$ potentiation is dependent on Ca^{2+}/calmodulin (CaM) pathway (Fig. 4) is consistent with the previous report that Ca^{2+}/CaM selectively modulates Nav1.6 currents (25). I showed that $I_{Na,P}$ potentiation increases the amplitude of EPSPs at subthreshold levels (Fig. 2), suggesting the distinctive role of $I_{Na,P}$ from fast

Na^+ currents. Possibly, a more hyperpolarized voltage threshold for Nav1.6 activation compared with other Na channel isoforms (63) may underlie the role of dendritic $I_{Na,P}$ as a regulator for subthreshold EPSPs.

Dendritic persistent sodium current and advancement of spike timing

In the present study, I demonstrate that mGluR5-mediated enhancement of dendritic $I_{Na,P}$ contributes to advancing AP initiation and increasing temporal precision of AP firing (Fig. 9). These results have major implications for spatial memory and spatial navigation. When hippocampal place cells increase their firing rates while the rat approaches and passes the cell's place field, spike timing gradually shifts to earlier phases of the theta cycle, which is known as phase precession or phase advance (64, 65). The phase relationship of the spike to the theta cycle is a good predictor of the rat's position in space (66, 67). Phase precession may be caused by the increased synaptic input in the place field, but the exact amount of synaptic inputs required to produce phase advancement could be regulated by dendritic voltage-gated ion channels, such as H-channels (68). I found that advancement of AP initiation also occurred when 5-Hz sine wave currents were injected (Fig. 2C), suggesting a possibility that enhancement of dendritic $I_{Na,P}$ may contribute to dendritic mechanisms of phase precession (68). Furthermore, the intrinsic ability of $I_{Na,P}$ in the dendrites to increase temporal precision (Fig. 9) may also have functional significance.

However, it should be noted that the absence of $I_{Na,P}$ in CA1-PNs has been shown to contribute to E-S precision (58). Vervaeke et al. reported that somatic $I_{Na,P}$ amplifies AHP and increases spike regularity during repetitive firing, but reduces the gain in discharge frequency and spike timing precision. The apparent difference in the roles of $I_{Na,P}$ in excitability may be due to the source of $I_{Na,P}$ in CA1-PNs. Vervaeke et al. used dynamic clamp method to selectively manipulate perisomatic $I_{Na,P}$, whereas in our experiment, bath application of DHPG or HFS at CA3-CA1 synapses selectively activate mGluR5 signaling in the proximal apical dendrites of CA1-PNs, which induces an increase in dendritic $I_{Na,P}$. Therefore, the different phenotypic consequences of spiking activity after an increase in $I_{Na,P}$ might be largely due to their differential subcellular localizations.

Ionic mechanism of mGluR5-mediated effects

I demonstrated that the intrinsic excitability of CA1-PNs is greatly enhanced by DHPG. Two key effects of group I mGluR on CA1 pyramidal neuron excitability were the increased AP frequency in response to long depolarization and the generation of mADP after repetitive firing (Fig. 10). I found that both effects are almost completely abolished by inhibition of Ca^{2+} release from ryanodine-sensitive stores or CaM and intracellular BAPTA, but not by EGTA (Fig. 14). Therefore, I propose that the target channels involved in increasing firing rate and the generation of mADP are both in close proximity to RyR and regulated by local Ca^{2+}. My recent work (22) and the present results provided

solid evidence that enhanced dendritic $I_{Na,P}$ induced by either mGluR5 agonist or HFS at CA3-CA1 synapses plays a significant role in the increase in firing rate and the improvement of spike timing precision. However, mGluR5-mediated mADP generation was not occluded by the blockade of $I_{Na,P}$, suggesting that the frequency changes and the generation of mADP might be operated by different target ion channels, despite the shared involvement of cADPR-RyR signaling pathways (Fig. 14). Furthermore, I observed that HFS at CA3-CA1 synapses fully reproduced mGluR5-dependent frequency changes, but not mADP generation. Local puff application of DHPG from soma to distal dendrite (Fig. 13) suggests that target ion channels underlying mGluR5-induced mADP are localized preferentially to the distal dendritic region. Taken together, these results suggest a compartmentalized distribution of ion channels responsible for distinct functions of mGluR5 activation. Overall, my results are in agreement with the subcellular distribution of the Nav1.6 subunit in CA1-PN dendrite, especially in proximal dendrites (17), however, it is important to note that Nav1.6 is also concentrated at the axon initial segment (AIS) in CA1-PNs (21, 69). Despite the abundance of a Nav1.6 expression at the AIS, selective activation of somatic mGluR5-signaling (Fig. 11A) or the local application of riluzole to the soma in the presence of DHPG in the bath (Fig. 12E) did not cause any changes in AP firing frequency. The reason why Nav1.6 in the AIS is not regulated by mGluR5 signaling remains to be examined. Together, my data suggest that the impact of mGluR5 signaling on CA1-PNs are highly complex and variety of ion channels are recruited upon their differential subcellular localizations.

Dendritic mGluR signaling

Previous study demonstrated that mGluR5-dependent Ca^{2+} release induced by mGluR agonist is independent of PLC/IP3 pathways and identified cADPR as a signaling molecule that activates ryanodine receptors (70). In the present paper, I found that the same signaling pathway underlies Ca^{2+} release induced by synaptically-activated mGluR5 in the dendrites of CA1-PNs (Fig. 3). In addition, I showed that potentiation of $I_{Na,P}$ and PT-ESP, which are downstream events of mGluR5-mediated Ca^{2+} release, are also independent of PLC/IP3 pathways but are mediated by cADPR/RyR signaling pathways (Fig. 4).

Ca^{2+} release by group I mGluR activation is generally believed to be mediated by PLC/IP3 pathway. This knowledge is based on the report by Nakamura et al (32), but they also showed that mGluR-dependent Ca^{2+} release at CA1 apical dendrites was abolished in the presence of ryanodine. However, they regarded this result as a manifestation of communication between RyR-sensitive store and IP3-sensitive store. Without testing the effect of PLC inhibitors, they reported that intracellular heparin prevented Ca^{2+} release, and concluded that Ca^{2+} release is IP3-dependent. I do not know the reason for the discrepancy for heparin effects, but found a clue in their result. They described that intracellular heparin did not block the slow depolarization. Considering that group I mGluR-induced slow depolarization is mediated by Ca^{2+} wave-dependent activation of TRPC (13), blocking Ca^{2+} release should block depolarization. Possibly, heparin may interfere Ca^{2+} measurement under certain experimental conditions (71). Such possibility needs to be carefully examined

to use heparin in Ca^{2+} measurement study as a selective blocker for IP3-dependent Ca^{2+} release. I suggest that to provide evidence for the IP3-dependence of Ca^{2+} release, the effect of PLC inhibition is also required. I showed that mGluR-mediated Ca^{2+} release is unaffected by PLC inhibition using not only pharmacological blockers but also PLC knockout mouse (70).

In CA1-PNs, a low-frequency stimulation for a long duration (3 Hz for 5 min) that induces synaptic LTD induced a long-term increase in intrinsic excitability because of the decrease in I_h currents, and these changes were mGluR dependent and Ca^{2+} dependent (5). I showed that HFS to the proximal apical dendrites modulates dendritic $I_{Na,P}$ but did not find any signature for changes in I_h (RMP and input resistance remained unchanged after HFS). Possibly, depending on the stimulation pattern, duration, and location, mGluR-mediated Ca^{2+} signaling may couple to different downstream events, resulting in different effects that last for different durations. Therefore, the roles of mGluR5-dependent short-term E-S potentiation in the hippocampal information processing are fundamental questions that remain to be answered in future studies.

Localization of mGluR5 and Nav1.6

The new form of E-S potentiation introduced in this study is highly dependent on the region along the proximodistal axis of the dendrites. The E-S potentiation is activated by mGluR5-signalling cascade and required upregulated Nav1.6 at

proximal region of CA1- PN dendrites. In hippocampus, mGluR5 is mainly expressed in dendritic fields of the stratum radiatum, whereas mGluR1 is mostly found on cell bodies. Subcellularly, group 1 mGluRs are localized postsynaptically in a perisynaptic zone surrounding the ionotropic receptors (18). A local application study shows that DHPG sensitive receptors are primarily located in distal dendrite (Fig. 13C). Moreover, Ca^{2+} signals evoked by mGluRs activation are also observed in CA1-PN distal dendrite (>250 μm, unpublished observations), implicating the presence of the mGluRs on distal dendrites as well as proximal dendrites. However, HFS to the distal synapses did not induce E-S potentiation (Fig. 7Ba, Bb, and C). Interestingly, enhanced mGluR5-dependent Nav1.6 activity is also required for the E-S potentiation. It is important to emphasize that a gradual decrease in Nav1.6 density along the proximodistal axis of the CA1 dendrite has been described by EM immunolocalization study (17). Although indirectly tested the interaction between mGluR5 and Nav1.6 with Ca^{2+} buffers (Fig. 14F, G, H), a direct evidence between mGluRs and Nav1.6 during the E-S potentiation is unknown. Therefore, it will be important to test how mGluRs and Nav1.6 are activated together in a restricted region of the neuron during E-S potentiation.

Functional implication of mGluR5-signaling

Two recent studies have found that cells with an increased intrinsic excitability before exposure to a novel environment were likely to become place cells (26,

27). Because synaptic plasticity-inducing events are not required for the formation of place cells in novel environment (27), differences in intrinsic excitability could be the cellular substrate for place field formation in CA1-PNs (26, 27). Generally, the intrinsic excitability is a major component determining the input-output functions, therefore, better knowledge about regulation rules of intrinsic excitability and modulatory influences that reshape the input-output function in CA1-PNs is essential for understanding the mechanism of place field formation. Our findings reveal that HFS-induced mGluR5 signaling, which induces potentiation of $I_{Na,P}$, transiently increases the gain of input-output functions in the absence of sustained synaptic inputs, and therefore this mGluR5-activated increase in dendritic excitability may support those two in vivo evidence (26, 27) showing that modulation of intrinsic properties of CA1-PN dendrites determines whether a pyramidal cell become a place cell or not.

Functional implication of mGluR5-meditated regulation on neuronal excitability

Although Group I mGluRs are known to facilitate or induce both long-term depression (LTD) and potentiation (LTP) of synaptic strength (72, 73), the best characterized synaptic plasticity induced by Group I mGluR is an mGluR-LTD of excitatory synaptic strength. To maintain modifiable synapses of a neuronal network within their optimal working range, the positive feedback mechanism of Hebbian plasticity should be stabilized by regulatory processes. In the

present study, I excluded both NMDA and $GABA_A$ receptor dependent modifications to isolate metabotropic glutamate receptor dependent plasticity. By lowering spike threshold, potentiation of $I_{Na,P}$ changes dendritic integration so that mGuR-LTD may be accompanied by an enhancement of overall spike output of the neuron. This harmony may contribute to maintain neuronal output at a similar mean level after mGluR-LTD, and this regulation of systemic valance may contribute a global homeostatic regulation of activity, preventing neuronal hypoexcitability. Therefore, an mGluR-LTD together with enhanced $I_{Na,P}$ -dependent excitability after correlated synaptic input may act synergistically to normalize output firing of a neuron and thus stabilize neuronal network.

REFERENCES

1. Bliss TV & Lomo T (1973) Long-lasting potentiation of synaptic transmission in the dentate area of the anaesthetized rabbit following stimulation of the perforant path. *J Physiol* 232(2):331-356.
2. Zhang W & Linden DJ (2003) The other side of the engram: experience-driven changes in neuronal intrinsic excitability. *Nat Rev Neurosci* 4(11):885-900.
3. Frick A, Magee J, & Johnston D (2004) LTP is accompanied by an enhanced local excitability of pyramidal neuron dendrites. *Nat Neurosci* 7(2):126-135.
4. Fan Y*, et al.* (2005) Activity-dependent decrease of excitability in rat hippocampal neurons through increases in I(h). *Nat Neurosci* 8(11):1542-1551.
5. Brager DH & Johnston D (2007) Plasticity of intrinsic excitability during long-term depression is mediated through mGluR-dependent changes in I(h) in hippocampal CA1 pyramidal neurons. *J Neurosci* 27(51):13926-13937.
6. Losonczy A, Makara JK, & Magee JC (2008) Compartmentalized dendritic plasticity and input feature storage in neurons. *Nature* 452(7186):436-441.
7. Spruston N (2008) Pyramidal neurons: dendritic structure and synaptic integration. *Nat Rev Neurosci* 9(3):206-221.
8. Major G, Larkum ME, & Schiller J (2013) Active properties of

neocortical pyramidal neuron dendrites. *Annu Rev Neurosci* 36:1-24.

9. Breakwell NA, Rowan MJ, & Anwyl R (1996) Metabotropic glutamate receptor dependent EPSP and EPSP-spike potentiation in area CA1 of the submerged rat hippocampal slice. *J Neurophysiol* 76(5):3126-3135.

10. Congar P, Leinekugel X, Ben-Ari Y, & Crepel V (1997) A long-lasting calcium-activated nonselective cationic current is generated by synaptic stimulation or exogenous activation of group I metabotropic glutamate receptors in CA1 pyramidal neurons. *J Neurosci* 17(14):5366-5379.

11. Chuang SC, Bianchi R, & Wong RK (2000) Group I mGluR activation turns on a voltage-gated inward current in hippocampal pyramidal cells. *J Neurophysiol* 83(5):2844-2853.

12. Sohn JW*, et al.* (2007) Receptor-specific inhibition of GABAB-activated K+ currents by muscarinic and metabotropic glutamate receptors in immature rat hippocampus. *J Physiol* 580(Pt. 2):411-422.

13. El-Hassar L, Hagenston AM, D'Angelo LB, & Yeckel MF (2011) Metabotropic glutamate receptors regulate hippocampal CA1 pyramidal neuron excitability via Ca(2)(+) wave-dependent activation of SK and TRPC channels. *J Physiol* 589(Pt 13):3211-3229.

14. Hoffman DA, Magee JC, Colbert CM, & Johnston D (1997) K+ channel regulation of signal propagation in dendrites of hippocampal pyramidal neurons. *Nature* 387(6636):869-875.

15. Lai HC & Jan LY (2006) The distribution and targeting of neuronal voltage-gated ion channels. *Nat Rev Neurosci* 7(7):548-562.

16. Beck H & Yaari Y (2008) Plasticity of intrinsic neuronal properties in CNS disorders. *Nat Rev Neurosci* 9(5):357-369.

17. Lorincz A & Nusser Z (2010) Molecular identity of dendritic voltage-gated sodium channels. *Science* 328(5980):906-909.

18. Luscher C & Huber KM (2010) Group 1 mGluR-dependent synaptic long-term depression: mechanisms and implications for circuitry and disease. *Neuron* 65(4):445-459.

19. Crill WE (1996) Persistent sodium current in mammalian central neurons. *Annu Rev Physiol* 58:349-362.

20. Bean BP (2007) The action potential in mammalian central neurons. *Nat Rev Neurosci* 8(6):451-465.

21. Royeck M*, et al.* (2008) Role of axonal NaV1.6 sodium channels in action potential initiation of CA1 pyramidal neurons. *J Neurophysiol* 100(4):2361-2380.

22. Yu W*, et al.* (2018) mGluR5-dependent modulation of dendritic excitability in CA1 pyramidal neurons mediated by enhancement of persistent Na(+) currents. *J Physiol* 596(17):4141-4156.

23. Carter BC, Giessel AJ, Sabatini BL, & Bean BP (2012) Transient sodium current at subthreshold voltages: activation by EPSP waveforms. *Neuron* 75(6):1081-1093.

24. Topolnik L, Chamberland S, Pelletier JG, Ran I, & Lacaille JC (2009) Activity-Dependent Compartmentalized Regulation of Dendritic Ca2+ Signaling in Hippocampal Interneurons. *Journal of Neuroscience* 29(14):4658-4663.

25. Herzog RI, Liu C, Waxman SG, & Cummins TR (2003) Calmodulin binds to the C terminus of sodium channels Nav1.4 and Nav1.6 and differentially modulates their functional properties. *J Neurosci* 23(23):8261-8270.

26. Lee D, Lin BJ, & Lee AK (2012) Hippocampal place fields emerge upon single-cell manipulation of excitability during behavior. *Science* 337(6096):849-853.

27. Cohen JD, Bolstad M, & Lee AK (2017) Experience-dependent shaping of hippocampal CA1 intracellular activity in novel and familiar environments. *Elife* 6.

28. Sheffield MEJ, Adoff MD, & Dombeck DA (2017) Increased Prevalence of Calcium Transients across the Dendritic Arbor during Place Field Formation. *Neuron* 96(2):490-504 e495.

29. Schmidt-Hieber C & Nolan MF (2017) Synaptic integrative mechanisms for spatial cognition. *Nat Neurosci* 20(11):1483-1492.

30. Csicsvari J, Hirase H, Mamiya A, & Buzsaki G (2000) Ensemble patterns of hippocampal CA3-CA1 neurons during sharp wave-associated population events. *Neuron* 28(2):585-594.

31. Lee SH, Park KH, Ho WK, & Lee SH (2007) Postnatal developmental changes in Ca2+ homeostasis in supraoptic magnocellular neurons. *Cell Calcium* 41(5):441-450.

32. Nakamura T, Barbara JG, Nakamura K, & Ross WN (1999) Synergistic release of Ca2+ from IP3-sensitive stores evoked by synaptic activation of mGluRs paired with backpropagating action potentials. *Neuron*

24(3):727-737.

33. Jia Z*, et al.* (1998) Selective abolition of the NMDA component of long-term potentiation in mice lacking mGluR5. *Learn Mem* 5(4-5):331-343.

34. Nakamura T*, et al.* (2000) Inositol 1,4,5-trisphosphate (IP3)-mediated Ca2+ release evoked by metabotropic agonists and backpropagating action potentials in hippocampal CA1 pyramidal neurons. *J Neurosci* 20(22):8365-8376.

35. Ross WN (2012) Understanding calcium waves and sparks in central neurons. *Nat Rev Neurosci* 13(3):157-168.

36. Sohn JW*, et al.* (2011) Cyclic ADP Ribose-Dependent Ca Release by Group I Metabotropic Glutamate Receptors in Acutely Dissociated Rat Hippocampal Neurons. *PLoS One* 6(10):e26625.

37. Kim Y, Hsu CL, Cembrowski MS, Mensh BD, & Spruston N (2015) Dendritic sodium spikes are required for long-term potentiation at distal synapses on hippocampal pyramidal neurons. *Elife* 4.

38. Madeja M (2000) Do neurons have a reserve of sodium channels for the generation of action potentials? A study on acutely isolated CA1 neurons from the guinea-pig hippocampus. *Eur J Neurosci* 12(1):1-7.

39. Park JY*, et al.* (2010) A post-burst after depolarization is mediated by group i metabotropic glutamate receptor-dependent upregulation of Ca(v)2.3 R-type calcium channels in CA1 pyramidal neurons. *PLoS Biol* 8(11):e1000534.

40. D'Ascenzo M*, et al.* (2009) Activation of mGluR5 induces spike

afterdepolarization and enhanced excitability in medium spiny neurons of the nucleus accumbens by modulating persistent Na+ currents. *J Physiol* 587(Pt 13):3233-3250.

41. Lipowsky R, Gillessen T, & Alzheimer C (1996) Dendritic Na+ channels amplify EPSPs in hippocampal CA1 pyramidal cells. *J Neurophysiol* 76(4):2181-2191.

42. Yue C, Remy S, Su H, Beck H, & Yaari Y (2005) Proximal persistent Na+ channels drive spike afterdepolarizations and associated bursting in adult CA1 pyramidal cells. *J Neurosci* 25(42):9704-9720.

43. Urbani A & Belluzzi O (2000) Riluzole inhibits the persistent sodium current in mammalian CNS neurons. *Eur J Neurosci* 12(10):3567-3574.

44. van Drongelen W*, et al.* (2006) Role of persistent sodium current in bursting activity of mouse neocortical networks in vitro. *J Neurophysiol* 96(5):2564-2577.

45. Hutcheon B & Yarom Y (2000) Resonance, oscillation and the intrinsic frequency preferences of neurons. *Trends Neurosci* 23(5):216-222.

46. Hu H, Vervaeke K, Graham LJ, & Storm JF (2009) Complementary theta resonance filtering by two spatially segregated mechanisms in CA1 hippocampal pyramidal neurons. *J Neurosci* 29(46):14472-14483.

47. Sidiropoulou K*, et al.* (2009) Dopamine modulates an mGluR5-mediated depolarization underlying prefrontal persistent activity. *Nat Neurosci* 12(2):190-199.

48. Sourdet V, Russier M, Daoudal G, Ankri N, & Debanne D (2003) Long-term enhancement of neuronal excitability and temporal fidelity

mediated by metabotropic glutamate receptor subtype 5. *J Neurosci* 23(32):10238-10248.

49. Guerineau NC, Gahwiler BH, & Gerber U (1994) Reduction of resting K+ current by metabotropic glutamate and muscarinic receptors in rat CA3 cells: mediation by G-proteins. *J Physiol* 474(1):27-33.

50. Cudmore RH & Turrigiano GG (2004) Long-term potentiation of intrinsic excitability in LV visual cortical neurons. *J Neurophysiol* 92(1):341-348.

51. Spitzer NC (1991) A developmental handshake: neuronal control of ionic currents and their control of neuronal differentiation. *J Neurobiol* 22(7):659-673.

52. Mongillo G, Barak O, & Tsodyks M (2008) Synaptic theory of working memory. *Science* 319(5869):1543-1546.

53. Bliss TV & Collingridge GL (1993) A synaptic model of memory: long-term potentiation in the hippocampus. *Nature* 361(6407):31-39.

54. Dudman JT, Tsay D, & Siegelbaum SA (2007) A role for synaptic inputs at distal dendrites: instructive signals for hippocampal long-term plasticity. *Neuron* 56(5):866-879.

55. Jarsky T, Roxin A, Kath WL, & Spruston N (2005) Conditional dendritic spike propagation following distal synaptic activation of hippocampal CA1 pyramidal neurons. *Nat Neurosci* 8(12):1667-1676.

56. Takahashi H & Magee JC (2009) Pathway interactions and synaptic plasticity in the dendritic tuft regions of CA1 pyramidal neurons. *Neuron* 62(1):102-111.

57. Magee JC & Johnston D (1997) A synaptically controlled, associative signal for Hebbian plasticity in hippocampal neurons. *Science* 275(5297):209-213.

58. Vervaeke K, Hu H, Graham LJ, & Storm JF (2006) Contrasting effects of the persistent Na+ current on neuronal excitability and spike timing. *Neuron* 49(2):257-270.

59. Stuart G & Sakmann B (1995) Amplification of EPSPs by axosomatic sodium channels in neocortical pyramidal neurons. *Neuron* 15(5):1065-1076.

60. Branco T*, et al.* (2016) Near-Perfect Synaptic Integration by Nav1.7 in Hypothalamic Neurons Regulates Body Weight. *Cell* 165(7):1749-1761.

61. Baker MD (2005) Protein kinase C mediates up-regulation of tetrodotoxin-resistant, persistent Na+ current in rat and mouse sensory neurones. *J Physiol* 567(Pt 3):851-867.

62. Harvey PJ, Li X, Li Y, & Bennett DJ (2006) 5-HT2 receptor activation facilitates a persistent sodium current and repetitive firing in spinal motoneurons of rats with and without chronic spinal cord injury. *J Neurophysiol* 96(3):1158-1170.

63. Rush AM, Dib-Hajj SD, & Waxman SG (2005) Electrophysiological properties of two axonal sodium channels, Nav1.2 and Nav1.6, expressed in mouse spinal sensory neurones. *J Physiol* 564(Pt 3):803-815.

64. O'Keefe J & Recce ML (1993) Phase relationship between

hippocampal place units and the EEG theta rhythm. *Hippocampus* 3(3):317-330.

65. Skaggs WE, McNaughton BL, Wilson MA, & Barnes CA (1996) Theta phase precession in hippocampal neuronal populations and the compression of temporal sequences. *Hippocampus* 6(2):149-172.

66. Jensen O & Lisman JE (2000) Position reconstruction from an ensemble of hippocampal place cells: contribution of theta phase coding. *J Neurophysiol* 83(5):2602-2609.

67. Tsodyks MV, Skaggs WE, Sejnowski TJ, & McNaughton BL (1996) Population dynamics and theta rhythm phase precession of hippocampal place cell firing: a spiking neuron model. *Hippocampus* 6(3):271-280.

68. Magee JC (2001) Dendritic mechanisms of phase precession in hippocampal CA1 pyramidal neurons. *J Neurophysiol* 86(1):528-532.

69. Hsu CL, Zhao X, Milstein AD, & Spruston N (2018) Persistent Sodium Current Mediates the Steep Voltage Dependence of Spatial Coding in Hippocampal Pyramidal Neurons. *Neuron* 99(1):147-162 e148.

70. Sohn JW*, et al.* (2011) Cyclic ADP ribose-dependent Ca2+ release by group I metabotropic glutamate receptors in acutely dissociated rat hippocampal neurons. *PLoS One* 6(10):e26625.

71. Landt M, Hortin GL, Smith CH, McClellan A, & Scott MG (1994) Interference in ionized calcium measurements by heparin salts. *Clin Chem* 40(4):565-570.

72. Anwyl R (1999) Metabotropic glutamate receptors:

electrophysiological properties and role in plasticity. *Brain Res Brain Res Rev* 29(1):83-120.

73. Bellone C, Luscher C, & Mameli M (2008) Mechanisms of synaptic depression triggered by metabotropic glutamate receptors. *Cell Mol Life Sci* 65(18):2913-2923.

국문초록

피라미드 세포의 수상돌기에 존재하는 나트륨 채널은 시냅스 신호를 증폭시켜 활동전위의 발생을 촉진시킨다고 알려져 있다. 그러나 수상돌기 나트륨 채널이 조절되는 기작은 거의 알려져 있지 않다. 본 저자는 이번 연구에서, 해마 흥분성 시냅스 신호를 CA1 피라미드 신경세포 (CA1-PNs)의 근거리 수상돌기에 줄 때, 수상돌기의 흥분성이 일시적으로 증가하는 새로운 종류의 단기 시냅스 가소성에 대해서 보고한다. 고빈도 자극 (HFS)을 Schaffer collateral (SC) 경로에 줄 때, CA1-PNs의 수상돌기에서 대사성 글루탐산 수용체5 (mGluR5) 의존적인 칼슘 신호전달이 활성화되고, 칼모듈린 신호전달경로를 거쳐서 Nav1.6 채널과 관련된 지속 나트륨 전류 ($I_{Na,P}$)를 증가시킨다. HFS에 의한 수상돌기 $I_{Na,P}$ 증가를 통해 흥분성 시냅스 후 전위 (EPSP)가 일시적으로 증가하는데, 이러한 현상은 HFS를 근거리 수상돌기에 줄 때 뿐 아니라 원거리 수상돌기에 줄 때에도 관찰된다. 이 때, 활동전위 역치가 감소되어 활동전위 발생빈도가 증가하고, 활동전위 발생 속도가 증가하며, 활동전위 발생의 정확도와 발생시기도 단축된다. 종합적으로, 본 저자는 수상돌기의 $I_{Na,P}$가 활동 의존적으로 수지상 집적화를 조절하고, 또한 신경세포의 출력을 조절하는데 관여하는 새로운 타겟임을 발견했다. 한편, 생리자극과 동일한 정도의 고빈도 자극을 CA1-CA3 시냅스에 줄 때에도

mGluR5이 활성화 되는데, 이 때 mGluR5에 의해 증가한 CA1-PNs 수상돌기의 $I_{Na,P}$는 해마의 place field 형성을 이해하는데 중요한 단서가 될 수 있다.

중심단어: mGluR5 의존적 가소성, CA1 피라이드 뉴런, 내재적 흥분성, 고빈도 자극

학번: 2009-21894